

University of Windsor

Scholarship at UWindor

Electronic Theses and Dissertations

Theses, Dissertations, and Major Papers

9-27-2023

Electromagnetically Induced Transparency in an Ensemble of Three-Level Lambda Systems

Sara Moezzi
University of Windsor

Follow this and additional works at: <https://scholar.uwindsor.ca/etd>



Part of the [Quantum Physics Commons](#)

Recommended Citation

Moezzi, Sara, "Electromagnetically Induced Transparency in an Ensemble of Three-Level Lambda Systems" (2023). *Electronic Theses and Dissertations*. 9252.
<https://scholar.uwindsor.ca/etd/9252>

This online database contains the full-text of PhD dissertations and Masters' theses of University of Windsor students from 1954 forward. These documents are made available for personal study and research purposes only, in accordance with the Canadian Copyright Act and the Creative Commons license—CC BY-NC-ND (Attribution, Non-Commercial, No Derivative Works). Under this license, works must always be attributed to the copyright holder (original author), cannot be used for any commercial purposes, and may not be altered. Any other use would require the permission of the copyright holder. Students may inquire about withdrawing their dissertation and/or thesis from this database. For additional inquiries, please contact the repository administrator via email (scholarship@uwindsor.ca) or by telephone at 519-253-3000ext. 3208.

Electromagnetically Induced Transparency in an Ensemble of Three-Level Lambda Systems

By

Sara Moezzi

A Thesis

Submitted to the Faculty of Graduate Studies through the Department of Physics
in Partial Fulfillment of the Requirements for
the Degree of Master of Science
at the University of Windsor

Windsor, Ontario, Canada

2023

© 2023 Sara Moezzi

Electromagnetically Induced Transparency in an Ensemble of Three-Level Lambda Systems

by

Sara Moezzi

APPROVED BY:

P. Moradian Zadeh
School of Computer Science

J. Rau
Department of Physics

C. Rangan, Advisor
Department of Physics

9 August 2023

Declaration of Originality

I hereby certify that I am the sole author of this thesis and that no part of this thesis has been published or submitted for publication.

I certify that, to the best of my knowledge, my thesis does not infringe upon anyone's copyright nor violate any proprietary rights and that any ideas, techniques, quotations, or any other material from the work of other people included in my thesis, published or otherwise, are fully acknowledged in accordance with the standard referencing practices. Furthermore, to the extent that I have included copyrighted material that surpasses the bounds of fair dealing within the meaning of the Canada Copyright Act, I certify that I have obtained written permission from the copyright owner(s) to include such material(s) in my thesis and have included copies of such copyright clearances to my appendix.

I declare that this is a true copy of my thesis and that this thesis has not been submitted for a higher degree to any other University or Institution.

Abstract

Electromagnetically induced transparency (EIT) is a technique whereby a medium otherwise opaque to radiation of a particular frequency can be made transparent at that frequency by applying radiation of an appropriate second frequency. EIT demonstrates numerous current applications, with a notable focus on its utilization within the field of quantum information. Given the absence of an established theory of EIT in atomic ensembles, my primary focus is to develop theoretical models that describe both the quantum mechanical origin of EIT as well as the effect of interatomic interactions.

In this thesis, I present two theoretical models of EIT in an ensemble of three-level atoms in a lambda configuration. The ensemble is modelled by a 5-level quantum system with the mean-field interactions between atoms modelled by decoherence terms. The dynamics of the ensemble are calculated by solving the Lindblad Master Equation for the density matrix. From the density matrix, the polarizability, and the frequency-dependence of the electric susceptibility and the group refractive index are calculated. A strong dependence on the density of the ensemble is observed.

Additionally, I explore the propagation of a Gaussian probe pulse within an atomic medium composed of three-level Λ systems (3LAS). By solving the coupled Maxwell and Liouville-von Neumann equations under the assumption of slow variations in the electric field across both space and time, I showed that intriguing results emerge, particularly concerning the influence of density on pulse dynamics.

Furthermore, comparing the two models over a range of ensemble number densities, it was seen that despite achieving a favorable transparency window by increasing the number density in the first model, the second model shows that EIT is not observed at high densities.

Acknowledgements

I would like to express my deep appreciation to my advisor, Dr. Chitra Rangan, for her patience, continuous motivation, and strong support during this journey. I have been really lucky to be a member of her research group and her encouragement has been instrumental in making this project a reality. I would like to thank my committee members, Dr. Jeffrey Rau, Dr. Pooya Moradian Zadeh and Dr. Tj Hammond, the chair of the committee, for their time, valuable suggestions, and providing insightful comments.

I am incredibly thankful to my family and friends for their constant love and support. Their presence in my life has been a source of immense joy and strength, and I feel truly blessed to have such wonderful people by my side. Their encouragement and belief in me have inspired me to pursue my dreams with confidence and determination. I am grateful for every moment we share together and for the countless memories we create.

This research was supported by the Natural Science and Engineering Research Council of Canada (NSERC), Discovery Grant (RGPIN-2019-66387). I want to sincerely thank them for their support. I am also grateful to the University of Windsor for financial support, which played a pivotal role in making this endeavor possible.

Table of Contents

Declaration of Originality	iii
Abstract	iv
Acknowledgements	v
List of Figures	viii
1 Introduction	1
2 EIT Overview	6
2.1 Lambda EIT Scheme	6
2.1.1 Lindblad-von Neumann Equation	8
2.1.2 Linear Susceptibility	11
2.2 Slow Light	14
3 Modelling a Dense Ensemble of 3-Level Λ systems	17
3.1 Maxwell–von Neumann Equations	17
3.2 Modeling an Ensemble of Atomic Systems with Directional Basis States . .	19
3.2.1 Two-Level Systems	19
3.2.2 Three-Level Λ Systems (3LAS)	21
3.3 Effective Single Particle Models of an Atomic Ensemble	22
3.3.1 Ensemble of Two-Level Atoms	22
3.3.2 Ensemble of 3-Level Λ Systems	27
4 Modelling EIT in an Atomic Ensemble	34
4.1 EIT in an Atomic Ensemble: Single Particle Model	34
4.1.1 Effect of Number Density	37
4.1.2 Effect of Control Field Strength and Spontaneous Emission	39
4.2 Modelling EIT in an Atomic Ensemble with a Pulsed Probe	41
5 Conclusion	49
5.1 Future Directions	50
5.2 Limitations	51
Appendix A The Interaction Picture with the Rotating Wave Approximation (RWA)	53
A.1 Three-level Λ Systems	54
A.2 Three-level Λ Systems with a Multi-directional excited state	55

Table of Contents	vii
Appendix B Lindblad-von Neumann Equation	56
Appendix C Scaling Parameters	59
Bibliography	60
Vita Auctoris	65

List of Figures

2.1	Schematic diagram of a three-level Λ -type atomic system.	7
2.2	The real and imaginary parts of the density matrix element ρ_{20} for $\Omega_p = 0.1\text{MHz}$, $\Omega_c = 1\text{MHz}$, $\gamma_0 = \gamma_1 = 3.03\text{MHz}$, $\Delta_p = -0.1\text{MHz}$ and $\Delta_c = 0$ in terms of time.	11
2.3	The real part of the density matrix element ρ_{22} for $\Omega_p = 0.1\text{MHz}$, $\Omega_c = 1\text{MHz}$, $\gamma_0 = \gamma_1 = 3.03\text{MHz}$, $\Delta_p = -0.1\text{MHz}$ and $\Delta_c = 0$ in terms of time.	12
2.4	The real and imaginary parts of the susceptibility for $\Omega_p = 0.1\text{MHz}$, $\gamma_0 = \gamma_1 = 3.03\text{MHz}$, $N = 10^{20}m^{-3}$, $\Delta_c = 0$ and $\Omega_c = 0$ in terms of the probe laser detuning.	13
2.5	The real and imaginary parts of the susceptibility for $\Omega_p = 0.1\text{MHz}$, $\gamma_0 = \gamma_1 = 3.03\text{MHz}$, $N = 10^{20}m^{-3}$, $\Delta_c = 0$ and $\Omega_c = 0$ in terms of the probe laser detuning.	14
2.6	The group index n_g of probe light for $\Omega_p = 0.1\text{MHz}$, $\gamma_0 = \gamma_1 = 3.03\text{MHz}$, $N = 10^{20}m^{-3}$ and $\Omega_c = 1\text{MHz}$ in terms of the probe laser detuning.	15
3.1	Schematic energy diagrams of a atomic system. a) The electric dipole moment of the two-level atom is oriented along the incident field polarization direction. b) The effective energy level structure of the two-level system that can be excited by the different field polarization components. Ω 's and Δ 's are the dipole-field interaction frequency and detuning, respectively. γ 's denote the spontaneous emission rates from the respective levels to the ground state	20
3.2	The effective energy level structure of the three-level Λ system that can be excited by the different field polarization components. ω_p and ω_c are the angular frequencies of the probe and control laser beams, respectively. Δ_p and Δ_c denote the detuning of the probe and the coupling fields with respect to their atomic transition energies.	21

3.3	A sketch of the transition structure in the effective single-particle model of the driven ensemble of atoms. The blue and red dashed curves correspond to the spontaneous emission and dephasing due to interatomic energy transfer.	24
3.4	Excited state populations of single particle model as a function of time for two values of number density of atoms in the ensemble. The amplitude of the driving electric field E is $1.5 \times 10^9 \text{V/m}$. Here we have set $\Delta = 0$.	27
3.5	A sketch of the transition structure in the effective single-particle model of the driven ensemble of atoms. The blue (orange) and red dashed curves correspond to the spontaneous emission and dephasing due to interatomic energy transfer.	28
4.1	The imaginary parts of the susceptibility χ_{py} for the single and effective single models with parameters $\Omega_{py} = 0.1 \text{MHz}$, $\Omega_{cy} = 1 \text{MHz}$, $\gamma_0 = \gamma_1 = 3.03 \text{MHz}$, $N = 10^{24} \text{m}^{-3}$ and $\Delta_c = 0$ in terms of the probe laser detuning.	36
4.2	The real parts of the susceptibility χ_{py} for the single and effective single models with parameters $\Omega_{py} = 0.1 \text{MHz}$, $\Omega_{cy} = 1 \text{MHz}$, $\gamma_0 = \gamma_1 = 3.03 \text{MHz}$, $N = 10^{24} \text{m}^{-3}$ and $\Delta_c = 0$ in terms of the probe laser detuning.	36
4.3	The group refractive index of probe light for the 3LAS and an ensemble of 3LAS as a function of Δ_p with $\Omega_{py} = 0.1 \text{MHz}$, $\Omega_{cy} = 1 \text{MHz}$, $\gamma_0 = \gamma_1 = 3.03 \text{MHz}$, $\Delta_c = 0$.	37
4.4	The imaginary parts of the susceptibility as a function of probe laser detuning for $\Omega_{py} = 0.1 \text{MHz}$, $\Omega_{cy} = 1 \text{MHz}$, $\gamma_0 = \gamma_1 = 3.03 \text{MHz}$, $\Delta_c = 0$ and various values of the number density N .	37
4.5	FWHM of the imaginary part of the susceptibility as a function of number density N for Fig. 4.4.	38
4.6	Populations ρ_{2x2x} and ρ_{2y2y} in in the x and y directional excited states as a function of number density N for Fig. 4.4.	38
4.7	The group index of probe light as a function of probe laser detuning for $\Omega_{py} = 0.1 \text{MHz}$, $\Omega_{cy} = 1 \text{MHz}$, $\gamma_0 = \gamma_1 = 3.03 \text{MHz}$, $\Delta_c = 0$ and various values of the number density N .	39
4.8	The imaginary parts of the susceptibility as a function of probe laser detuning for $\Omega_{py} = 0.1 \text{MHz}$, $\gamma_0 = \gamma_1 = 3.03 \text{MHz}$, $\Delta_c = 0$, $N = 10^{24}$ and various values of the control field Rabi frequency Ω_{cy} . The curves from top to down correspond to $\Omega_{cy} = 0.5, 1, 1.5, 2$ and 2.5MHz .	40

- 4.9 The rimaginary parts of the susceptibility as a function of probe laser detuning for $\Omega_{py} = 0.1\text{MHz}$, $\Omega_{cy} = 1\text{MHz}$, $\Delta_c = 0$, $N = 10^{24}\text{m}^{-3}$ and various values of the spontaneous emission $\gamma_0 = \gamma_1 = \gamma$. The curves from top to down correspond to $\gamma = 0.5, 1.5, 2.5$ and 3.5 MHz. 40
- 4.10 The probe laser field for the input and output pulses in all directions. The parameters used are $\Omega_{py0} = 0.1\text{MHz}$, $\Omega_{cy} = 1\text{MHz}$, $\gamma_0 = \gamma_1 = 3.03\text{MHz}$, $N = 10^{16}\text{m}^{-3}$, $\Delta_p = 0$, $\Delta_c = 0$, $\Delta\tau = 14.52\mu\text{s}$ and $L = 500\text{nm}$. The input and output pulses match with each other. Note that the scale of the y -axis in figures (b) and (c) is Hz. The scattering in the x and z directions is very small. 46
- 4.11 The probe laser field for the input and output pulses in all directions. The parameters used are $\Omega_{py0} = 0.1\text{MHz}$, $\Omega_{cy} = 1\text{MHz}$, $\gamma_0 = \gamma_1 = 3.03\text{MHz}$, $N = 10^{20}\text{m}^{-3}$, $\Delta_p = 0$, $\Delta_c = 0$, $\Delta\tau = 14.53\mu\text{s}$ and $L = 58.5\text{nm}$. The horizontal thin gray dashed line denotes $1/e$ of a maximum of the initial input pulse. 47
- 4.12 The behaviors of absorption length L_α versus number density N . The parameters used are $\Omega_{py0} = 0.1\text{MHz}$, $\Omega_{cy} = 1\text{MHz}$, $\gamma_0 = \gamma_1 = 3.03\text{MHz}$, $\Delta_p = 0$, $\Delta_c = 0$. We use the logarithmic scale for the vertical axis. 48

Chapter 1

Introduction

Electromagnetically induced transparency (EIT) is a quantum optics phenomenon in atomic systems with multilevel electronic structures that dramatically modifies the absorption and refractive index of a medium. EIT results from the coherent, quantum interference between two different excitation pathways to an excited state, rendering an initially opaque medium transparent to the probe field. The transparency occurs over a narrow spectral region within the broad absorption spectrum. The significant degree of transparency is accompanied by a strong decrease in group velocity so that the light inside the medium can be slowed down and even stopped [1].

Historically, the theoretical foundations of EIT were set forth by Kocharovskaya and Khanin [2] in 1988 and independently by Harris [3] in 1989. The first experimental observation of EIT was achieved in a strontium vapour by Harris et al. [4] in 1991. To date, the EIT effect is most commonly realized in three types of 3-level atomic configurations: known as Λ (Lambda) [1], Ξ (Ladder) [5, 6] and V (Vee) [7] systems. The Λ type is the simplest scheme and has been extensively studied in the literature. In this case, two lower energy levels are coupled to a single upper energy level by a coupling and a probe laser, and coherence is created between the two lower levels [1]. More intriguing is the behavior of the atomic systems interacting with multiple laser beams, for which more than one EIT window appears in the absorption spectrum [8, 9]. Multiple transparency windows have been reported in different multi-levels atomic systems, such as N -type [10, 11], Y -type [12, 13], K -type [14], W -type [15] and inverted Y -type [16, 17].

EIT experiments in atomic ensembles have been conducted at various temperatures. For example, the use of room temperature experimentation in an ensemble of atoms occurs in one study [5] that investigates EIT in a three-level system (Ladder type) in a Doppler-broadened medium, focusing closely on counterpropagating fields with similar frequencies to minimize the Doppler width. This study [5] extends the theory to include the lambda configuration and explores various regimes and optimization strategies for absorption reduction. When comparing this theory with the conducted experiment and the use of the Rb D2 line at room temperature [5], they are presented with good agreement and with noted limitations due to the linewidth of the diode lasers used. In another notable experiment at room temperature [18], EIT can be observed in a pure Rb vapour cell and Rb vapour filled with nitrogen (Rb–N₂) in a five-level lambda configuration. In this context, the presence of buffer gas in combination with the Rb vapour enhances the EIT contrast. Recent research has shifted its focus to explore EIT specifically in ensembles of cold atoms [19], presenting a notable departure from previous studies that predominantly utilized ensembles of warm atoms [20] or even including those conducted at room temperature [5]. Ahufinger et al. [19] examined the EIT absorption spectrum of the cold atoms between above and below the transition temperature for Bose–Einstein condensation.

The discovery of EIT in atomic ensembles has led to the development of significant scientific applications [1] including control of optical group delay in a medium [21], production of dark state polaritons [22, 23] and quantum memory [24].

- By using EIT, optical group delay can be controlled through the manipulation of the dispersion properties of an atomic medium. One study [21] examined the EIT region and found that the refractive index becomes extremely dispersive and changes depending on the frequency. This dispersion caused different frequency components of the probe field to experience different phase velocities and group velocities. The dispersion properties and affected optical group delay can be precisely controlled by manipulating the intensity and frequency of the control field [21].
- Dark state polaritons in EIT [22, 23] can be used in quantum optics and quantum information processing. Based on EIT, dark state polaritons can be formed by the coupling of the probe field with the collective atomic excitations in the system. This

happens while the control field is detuned from resonance.

- The concept of light storage and quantum memory within the transparency window in EIT was first presented in 2000 by Fleischhauer and Lukin [22]. In recent years, it has been proven that EIT with a strong control field enables the mapping of information from an input pulse into a collective atomic state. This information can be stored and eventually retrieved; effectively achieving light storage or quantum memory [24].

Research has revealed that EIT can be achieved in various systems: such as atomic vapors [5], semiconductor quantum wells [25], and semiconductor quantum dots [26]. The theory of EIT is established in the case of individual quantum emitters, such as atoms or molecules in dilute vapors [27, 28]. However, when dealing with two or more strongly interacting emitters or ensembles with high densities, the physics becomes significantly more complex. In these scenarios, the optical properties of an ensemble cannot be simply considered as the sum of their individual responses [29]. Collective effects arise due to the interactions among the quantum emitters within the system. Consequently, the total electric field experienced by an individual quantum emitter is the sum of both the applied field and the radiated field from all its neighbors [29].

Zhu (2016) [30] examined the impact of laser intensity, atomic density, and polarization on the optical response properties of a cold ensemble. In their study, they found that the atoms' motion can cause significant dephasing and diminish collective effects. Kuraptsev et al. (2014) [31], analyzed the spontaneous decay of a single atom inside cold atomic clouds for varying interatomic separation. They found that an atom inside the ensemble decays faster than a free atom. Sukharev (2011) [32] scrutinized the linear optical response of two-dimensional atomic clusters driven with low-intensity field for three-level atoms with two degenerate excited states. They found that atomic clusters have two well-distinguished resonances so that one resonant mode is located just below the atomic transition frequency of an individual atom, while the other is positioned significantly higher [32]. Diloreto (2018) [29] also investigated the dynamics of a dense three-dimensional ensemble of two-level quantum systems driven by a strong, linearly-polarized, plane wave electromagnetic field [29]. They showed that though the incident field is polarized in only a single direction, spontaneous emission from each atom may excite transitions in adjacent atoms in other

directions. Consequently, to fully capture interatomic interactions, the consideration of all three components of the dipole moment operator is required, where the three-excited basis is used for the quantum state of each emitter.

In this thesis, I set out to explore the EIT phenomena in an ensemble of atomic systems which are in a three-level Λ configuration with a multi-directional excited state. In particular, this model is constructed based on the nearest neighbor interatomic interaction of three-level Λ atoms in an ensemble. Each member of an ensemble acts as an individual quantum emitter that can spontaneously radiate field in all directions, even perpendicular to the direction of the incident beam. The radiation fields in all directions can excite atoms with different orientations of the dipole moment. I study the influence of these effects on the EIT behavior in an atomic ensemble which has not been considered in previous works. I analyze the optical properties of the ensemble and compare them to those of a single atom to gain a better understanding of how the ensemble's collective behavior affects EIT. In a second model, I investigated a Gaussian probe pulse propagating in a three-level Λ medium with a multi-directional excited state coupled to a monochromatic control field. This study has the promise of applications to improve optical quantum memory.

Thesis Overview

In this thesis, I study EIT in an ensemble of three-level Λ systems (3LAS). First, in Chapter 2, I review the theory of EIT in a single three-level Λ system, I show how we can calculate the electric susceptibility of the probe field through the density matrix. Then, I obtain the transparency window, and the group velocity for the probe field in the medium.

In Chapter 3, I show how to model an ensemble of atomic systems by using an effective single-particle model in which decoherence terms, such as effective spontaneous decay and dephasing rates are considered. With this methodology, I delve into the investigation of the EIT effect in the next chapter.

Finally, in Chapter 4, I extend the methodology of EIT modeling to an ensemble of 3LAS. I present two models. In the first model, I model the ensemble as a single particle density matrix with specific decoherence terms. With this model, I can predict the dependence of the transparency window and the group velocity of a probe field on the number density of an ensemble. I then extend a model of a probe field propagating through an ensemble in a

slowly varying (field) approximation. The dependence on density has interesting results.

Chapter 2

EIT Overview

In this chapter, I offer an overview of the theory of Electromagnetically Induced Transparency (EIT) in a single three-level quantum system in the Λ configuration. I start by obtaining both the steady-state and time dependent solutions of the Lindblad–von-Neumann equation for the density matrix. Then, I find a typical linear susceptibility spectrum for EIT in a Λ system. Lastly, I calculate transparency window and the group velocity of a probe field in an EIT medium.

2.1 Lambda EIT Scheme

The simplest configuration in which EIT can occur has three quantum Levels in a Λ configuration as in Fig.2.1. Here, two ground states $|0\rangle$ and $|1\rangle$ that are close in energy are connected to a single excited state $|2\rangle$ via a weak probe field and a strong control (signal) field, respectively. The transition $|0\rangle \leftrightarrow |1\rangle$ is a dipole forbidden transition. We use a semi-classical approach to describe the interaction of an atom with laser fields, where the atom and laser field are treated as a quantum mechanical object and a classical electric field, respectively.

The total Hamiltonian for the 3LAS

$$H = H_0 + H_1, \tag{2.1}$$

where H_0 is the Hamiltonian in the absence of the external laser field, consisting of the eigenstates $|0\rangle$, $|1\rangle$ and $|2\rangle$ with corresponding eigenvalue energies $\hbar\omega_0$, $\hbar\omega_1$ and $\hbar\omega_2$. H_0 is given in matrix form as

$$H_0 = \begin{pmatrix} \hbar\omega_0 & 0 & 0 \\ 0 & \hbar\omega_1 & 0 \\ 0 & 0 & \hbar\omega_2 \end{pmatrix}. \quad (2.2)$$

H_1 is the atom-field interaction Hamiltonian given by

$$H_1 = -\vec{\mu} \cdot \vec{E}, \quad (2.3)$$

in which $\vec{\mu}$ is the dipole moment operator and \vec{E} is applied electric field that is defined in the dipole approximation as

$$\vec{E} = \vec{\mathcal{E}}_p E_p \cos(\omega_p t) + \vec{\mathcal{E}}_c E_c \cos(\omega_c t). \quad (2.4)$$

Here, the weak probe field with an amplitude E_p , unit polarization vector $\vec{\mathcal{E}}_p$ and frequency

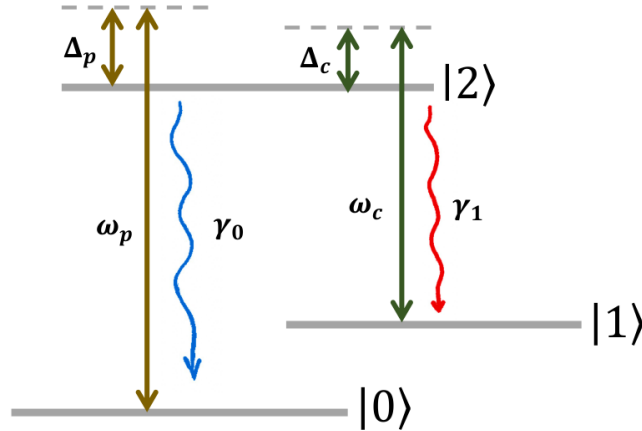


FIGURE 2.1: Schematic diagram of a three-level Λ -type atomic system.

ω_p couples the $|0\rangle \rightarrow |2\rangle$ transition, while the strong coupling field with an amplitude E_c , unit polarization vector $\vec{\mathcal{E}}_c$ and frequency ω_c drives the transition $|1\rangle \rightarrow |2\rangle$. Hence, the

matrix representation of the perturbation Hamiltonian is obtained as

$$H_1 = - \begin{pmatrix} 0 & 0 & \mu_{02}E_p \cos(\omega_p t) \\ 0 & 0 & \mu_{12}E_c \cos(\omega_c t) \\ \mu_{02}E_p \cos(\omega_p t) & \mu_{12}E_c \cos(\omega_c t) & 0 \end{pmatrix}, \quad (2.5)$$

where $\mu_{nm} = \mu_{mn} = \langle m | \mu | n \rangle$, ($m, n = 0, 1, 2$). The dipole moment matrix elements are assumed to be real. For convenience, H_1 is expressed in terms of exponents

$$H_1 = - \begin{pmatrix} 0 & 0 & \mu_{02}E_p(e^{-i\omega_p t} + e^{i\omega_p t})/2 \\ 0 & 0 & \mu_{12}E_c(e^{-i\omega_c t} + e^{i\omega_c t})/2 \\ \mu_{02}E_p(e^{-i\omega_p t} + e^{i\omega_p t})/2 & \mu_{12}E_c(e^{-i\omega_c t} + e^{i\omega_c t})/2 & 0 \end{pmatrix}. \quad (2.6)$$

2.1.1 Lindblad-von Neumann Equation

To find the dynamics of the system, one can employ the well-known density-matrix formalism. The time evolution of the density matrix ρ is described using the Lindblad-von Neumann equation [33]

$$\dot{\rho} = -\frac{i}{\hbar} [H, \rho] - L(\rho), \quad (2.7)$$

where the dot stands for the time derivative and $L(\rho)$ represents the Lindblad superoperator which has the form

$$L(\rho) = \sum_{d=0,1} \frac{\gamma_d}{2} \left(\sigma_d^\dagger \sigma_d \rho + \rho \sigma_d^\dagger \sigma_d - 2\sigma_d \rho \sigma_d^\dagger \right). \quad (2.8)$$

Here, σ_d are the Lindblad operators and γ_d is the atom spontaneous emission rate from $|2\rangle$ to $|0\rangle$ and $|1\rangle$. For a three-level Λ system, the spontaneous emission transition from $|1\rangle$ to $|0\rangle$ is dipole forbidden. The Lindblad operators σ_d are defined as follows

$$\sigma_0 = |0\rangle \langle 2|, \quad \sigma_1 = |1\rangle \langle 2|. \quad (2.9)$$

Briefly, by going into the interaction picture with unitary operator

$$U = \begin{pmatrix} e^{-i(\omega_p+\omega_2)t} & 0 & 0 \\ 0 & e^{-i(\omega_c+\omega_2)t} & 0 \\ 0 & 0 & e^{-i\omega_2 t} \end{pmatrix}, \quad (2.10)$$

and adopting the rotating wave approximation, where the counter-rotating terms are dropped, and by defining Rabi frequencies

$$\Omega_p = \frac{E_p \mu_{02}}{\hbar}, \quad \Omega_c = \frac{E_c \mu_{12}}{\hbar}, \quad (2.11)$$

the total Hamiltonian for the Λ system becomes

$$H_{RWA} = -\frac{\hbar}{2} \begin{pmatrix} -2\Delta_p & 0 & \Omega_p \\ 0 & -2\Delta_c & \Omega_c \\ \Omega_p & \Omega_c & 0 \end{pmatrix}, \quad (2.12)$$

in which $\Delta_p = \omega_p - \omega_2 + \omega_0$ and $\Delta_c = \omega_c - \omega_2 + \omega_1$ are the laser detunings. The details of the derivations are given in Appendix A.

So, the Lindblad-von Neumann equation becomes

$$\dot{\rho} = -\frac{i}{\hbar} [H_{RWA}, \rho] - L(\rho). \quad (2.13)$$

Note that the Lindblad-von Neumann equation 2.13 is written in the interaction picture as detailed in Appendix B, but the primes are dropped for convenience.

Writing the Lindblad-von Neumann equation Eq. 2.13 in component form, we have the diagonal elements

$$\begin{aligned} \dot{\rho}_{00} &= \gamma_0 \rho_{22} + \frac{1}{2} i \Omega_p (\rho_{20} - \rho_{02}), \\ \dot{\rho}_{11} &= \gamma_1 \rho_{22} + \frac{1}{2} i \Omega_c (\rho_{21} - \rho_{12}), \\ \dot{\rho}_{22} &= -(\gamma_0 + \gamma_1) \rho_{22} + \frac{1}{2} i \Omega_p (\rho_{02} - \rho_{20}) + \frac{1}{2} i \Omega_c (\rho_{12} - \rho_{21}), \end{aligned} \quad (2.14)$$

and the off-diagonal matrix elements

$$\begin{aligned}
\dot{\rho}_{01} &= i(\Delta_c - \Delta_p)\rho_{01} + \frac{1}{2}i\Omega_p\rho_{21} - \frac{1}{2}i\Omega_c\rho_{02}, \\
\dot{\rho}_{02} &= -\frac{1}{2}(2i\Delta_p + \gamma_0 + \gamma_1)\rho_{02} + \frac{1}{2}i\Omega_p(\rho_{22} - \rho_{00}) - \frac{1}{2}i\Omega_c\rho_{01}, \\
\dot{\rho}_{12} &= -\frac{1}{2}(2i\Delta_c + \gamma_0 + \gamma_1)\rho_{12} - \frac{1}{2}i\Omega_p\rho_{10} + \frac{1}{2}i\Omega_c(\rho_{22} - \rho_{11}). \tag{2.15}
\end{aligned}$$

The above equations are constrained by population conservation law $\rho_{00} + \rho_{11} + \rho_{22} = 1$ and the complex conjugate $\dot{\rho}_{ij} = \dot{\rho}_{ji}^*$. As it is apparent, the above equations are coupled to each other, and it is difficult to solve them analytically in general. In the following, we first obtain the analytic steady-state solution under the conditions that the system is initially in the ground state $|0\rangle$ and the probe field is very small in comparison to the coupling field, $\Omega_p \ll \Omega_c$. Additionally, we numerically solve the complete Lindblad-von Neumann equations Eqs. 2.14 and 2.15 without any simplifications. As we shall see next, one needs the density matrix element ρ_{02} in order to study EIT.

Steady-state Solution

In order to obtain the analytical solution for Eqs. 2.14 and 2.15, we assume that the system is initially in the ground state, i.e.,

$$\rho_{00} = 1, \quad \rho_{11} = 0, \quad \rho_{22} = 0. \tag{2.16}$$

By assuming a weak probe optical field, we perform a perturbation expansion of the set of Lindblad-von Neumann equations, Eqs. 2.14 and 2.15, up to first order in Ω_p . In the steady-state regime, the time derivative of each density matrix element vanishes and thus ρ_{02} can be readily calculated as [1]

$$\rho_{02} = \frac{2\Omega_p(\Delta_c - \Delta_p)}{2i(\Delta_c - \Delta_p)(\gamma_0 + \gamma_1 + 2i\Delta_p) - \Omega_c^2}. \tag{2.17}$$

In the next subsection, we will use the above relation to determine the linear susceptibility for a probe laser field.

Numerical Solution

Now, we solve numerically the Lindblad-von Neumann equation given by Eqs. 2.14

and 2.15 by using the NDSolve function of Wolfram Mathematica. One special aspect of NDSolve is its ability to analyze symbolic representations of both differential equations and solution domains. It then automatically picks the most appropriate numerical techniques based on the problem's inherent characteristics. Generally, a typical precision value in Mathematica's NDSolve is around 16.

To this end, we consider a 3LAS an alkali atom ^{87}Rb , where we set $|0\rangle = |5S_{1/2}, F = 1\rangle$, $|1\rangle = |5S_{1/2}, F = 2\rangle$ and $|2\rangle = |5P_{3/2}, F = 2\rangle$ [34]. The parameters we used in the numerical analysis are the following: $\Omega_p = 0.1\text{MHz}$, $\Omega_c = 1\text{MHz}$ and $\gamma_0 = \gamma_1 = 3.03\text{MHz}$. These parameters represent typical experimental values, with the Rabi frequencies being lower than the decoherence rates. By solving the time dependent Lindblad-von Neumann equation, we plot the real and imaginary parts of the density matrix element ρ_{20} as a function of time for $\Delta_p = 0.1\text{MHz}$ and $\Delta_c = 0$ in Fig. 2.2. It is noteworthy that at $t = 0$, all the atoms are initially in the ground state. As one can see from this figure, the time for the system to reach the steady state is about $t = 80\mu\text{s}$. Later using this data, one is able to numerically calculate the susceptibility. The excited-state population ρ_{22} as a function of time is obtained numerically and shown in Fig. 2.3.

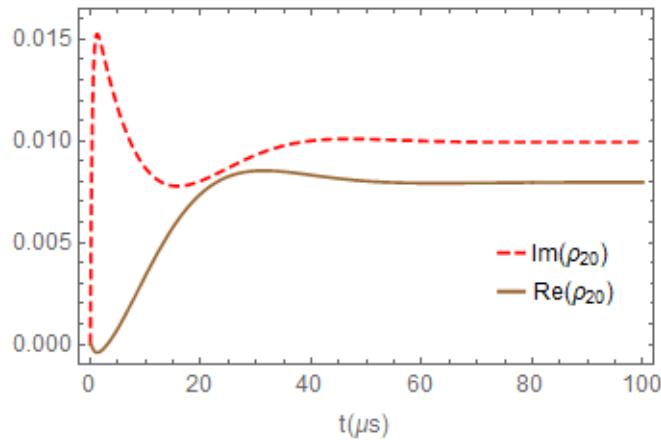


FIGURE 2.2: The real and imaginary parts of the density matrix element ρ_{20} for $\Omega_p = 0.1\text{MHz}$, $\Omega_c = 1\text{MHz}$, $\gamma_0 = \gamma_1 = 3.03\text{MHz}$, $\Delta_p = 0.1\text{MHz}$ and $\Delta_c = 0$ in terms of time.

2.1.2 Linear Susceptibility

To examine the optical response of a system, we need to know the absorption coefficient and refractive index profiles. These optical properties are related to the imaginary and real

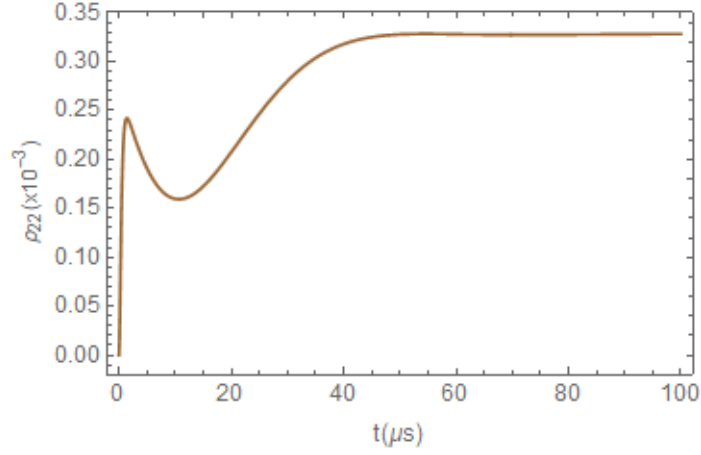


FIGURE 2.3: The real part of the density matrix element ρ_{22} for $\Omega_p = 0.1\text{MHz}$, $\Omega_c = 1\text{MHz}$, $\gamma_0 = \gamma_1 = 3.03\text{MHz}$, $\Delta_p = 0.1\text{MHz}$ and $\Delta_c = 0$ in terms of time.

parts of the electric susceptibility (χ) of the atomic medium by

$$\alpha = (\omega/c) \text{Im}(\chi), \quad n = 1 + \text{Re}(\chi)/2, \quad (2.18)$$

where c is the speed of light as well as α and n are the absorption coefficient and refractive index, respectively. In order to study EIT, one has to determine the electric susceptibility for the probe laser beam.

The induced linear polarization at the probe frequency ω_p is given by

$$P = \frac{1}{2} \epsilon_0 E_p [\chi_p(\omega_p) e^{-i\omega_p t} + \chi_p(\omega_p)^* e^{i\omega_p t}], \quad (2.19)$$

where ϵ_0 is the permittivity of vacuum and χ_p is the susceptibility of the atomic system due to the probe beam. On the other hand, by performing a quantum average of the dipole moment of the probe transition over an ensemble of N non-interacting atoms at the probe frequency ω_p , we have another expression for the polarization

$$\begin{aligned} P &= N \text{Tr}(\rho \mu) = N \sum_{i,j} \rho_{ij} \mu_{ji} \\ &= N \mu_{02} (\rho_{20} e^{-i\omega_p t} + \rho_{02} e^{i\omega_p t}), \end{aligned} \quad (2.20)$$

where ρ is the density matrix in the original untransformed frame. By comparing equations

2.19 and 2.20, the linear probe susceptibility in the limit $E_p \rightarrow 0$ is expressed as

$$\chi_p = \frac{2N\mu_{02}}{\epsilon_0 E_p} \rho_{20}. \quad (2.21)$$

According to the steady-state solution Eq. 2.17, the expression for the electric susceptibility is given by [1]

$$\chi_p = -\frac{2N\mu_{02}}{\epsilon_0 E_p} \frac{2\Omega_p(\Delta_c - \Delta_p)}{2i(\Delta_c - \Delta_p)(\gamma_0 + \gamma_1 - 2i\Delta_p) + \Omega_c^2}, \quad (2.22)$$

or equivalently

$$\chi_p = -\frac{2N\hbar}{\epsilon_0 E_p^2} \frac{2\Omega_p^2(\Delta_c - \Delta_p)}{2i(\Delta_c - \Delta_p)(\gamma_0 + \gamma_1 - 2i\Delta_p) + \Omega_c^2}, \quad (2.23)$$

in which we have used the Rabi frequencies formula, $\Omega_p = E_p\mu_{02}/\hbar$. When the control laser field is absent, $\Omega_c = 0$, the above susceptibility reduces to

$$\chi_p = \frac{2iN\hbar\Omega_p^2}{\epsilon_0 E_p^2 (\gamma_0 + \gamma_1 - 2i\Delta_p)}. \quad (2.24)$$

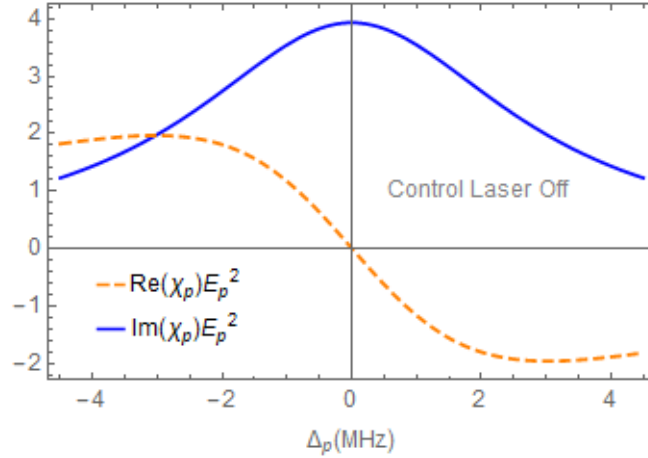


FIGURE 2.4: The real and imaginary parts of the susceptibility for $\Omega_p = 0.1\text{MHz}$, $\gamma_0 = \gamma_1 = 3.03\text{MHz}$, $N = 10^{20}\text{m}^{-3}$, $\Delta_c = 0$ and $\Omega_c = 0$ in terms of the probe laser detuning [34]. With the provided strength of the probe electric field, susceptibility values can be obtained.

The behavior of real and imaginary parts of susceptibility as a function of the probe laser detuning for the sample of alkali atom ^{87}Rb with the parameters $\Omega_p = 0.1\text{MHz}$, $\gamma_0 = \gamma_1 = 3.03\text{MHz}$, $\Delta_c = 0$ and $N = 10^{20}\text{m}^{-3}$ are depicted in Figs 2.4 and 2.5 for $\Omega_c = 0$ and $\Omega_c = 1\text{MHz}$. When the control laser is off ($\Omega_c = 0$), the probe field is absorbed very

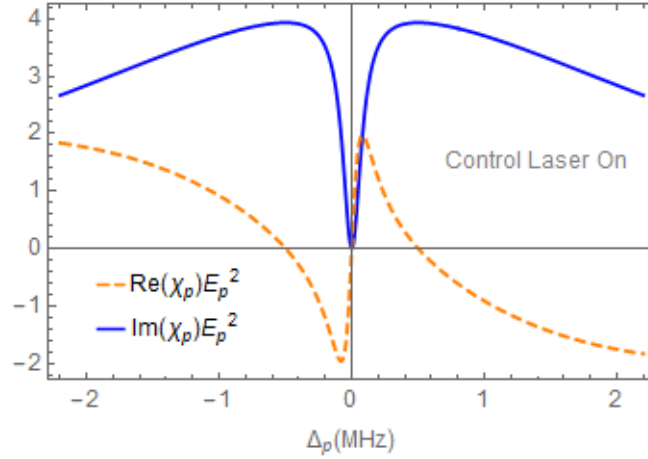


FIGURE 2.5: The real and imaginary parts of the susceptibility for $\Omega_p = 0.1\text{MHz}$, $\gamma_0 = \gamma_1 = 3.03\text{MHz}$, $N = 10^{20}\text{m}^{-3}$, $\Delta_c = 0$ and $\Omega_c = 1\text{MHz}$ in terms of the probe laser detuning. With the provided strength of the probe electric field, susceptibility values can be obtained.

strongly. When $\Omega_c \neq 0$, we can see that a transparency window is opened in the presence of the control beam at the probe frequency.

2.2 Slow Light

“Slow-light” [35] is an effect that accompanies EIT. When an optical beam propagates through a medium, its speed is changed by the interactions with the medium. Due to the dispersion effect, one can define the group velocity of the light as

$$v_g = \frac{d\omega}{dk} = \frac{c}{n_g}, \quad (2.25)$$

where c is the speed of light in vacuum, k is the wave number and n_g is the group refractive index at the optical frequency given by

$$n_g = n(\omega) + \omega \frac{dn(\omega)}{d\omega}. \quad (2.26)$$

Here, $n(\omega)$ is the refractive index which is a function of the real part of optical susceptibility (χ), $n = 1 + \text{Re}(\chi)/2$.

Obviously, the above relation Eq. (2.26) represents the dependency of v_g on $dn(\omega)/d\omega$ of the medium. Intuitively, $dn(\omega)/d\omega$ can have positive or negative values and the group index

could be larger or smaller than one. In particular, slow light occurs when $n_g \gg 1$ and fast light occurs when $n_g < 1$. Also, if $dn(\omega)/d\omega$ is sufficiently large and negative, n_g becomes negative. This negative group velocity is a special form of fast light, which is sometimes known as backwards light [36, 37]. The electromagnetically induced transparency (EIT) medium, which is optically controllable, is a standard way to create slow light [38–40].

According to the formula for electric susceptibility Eq. (2.23), the group index for the probe light in a three-level Λ EIT medium is given by the formula [35]

$$n_g = 1 - \frac{4\Gamma^2(4\Delta p^4 [2\Delta p + \omega_2] + \Delta p^2 \omega_2 2\Omega_c^2) - (\Omega_c^2 - 4\Delta p^2)^2 (4\Delta p^2 \omega_2 + [2\Delta p + \omega_2] \Omega_c^2)}{2^{-1} N^{-1} \hbar^{-1} \epsilon_0 E_p^2 \Omega_p^{-2} (4\Gamma^2 \Delta p^2 + [\Omega_c^2 - 4\Delta p^2]^2)^2}, \quad (2.27)$$

where we have assumed that $\Delta c = 0$ and $\Gamma \equiv \gamma_0 + \gamma_1$. At $\Delta p = 0$, all dependence on Γ is lost. The group index of probe light for the atomic medium of ^{87}Rb with the parameters $\Omega_p = 0.1\text{MHz}$, $\gamma_0 = \gamma_1 = 3.03\text{MHz}$ and $N = 10^{20}\text{m}^{-3}$ is shown in Fig. 2.6. We see that the largest reduction of group velocity is achieved at the resonance frequency, i.e. $\Delta p = 0$, where n_g is maximized.

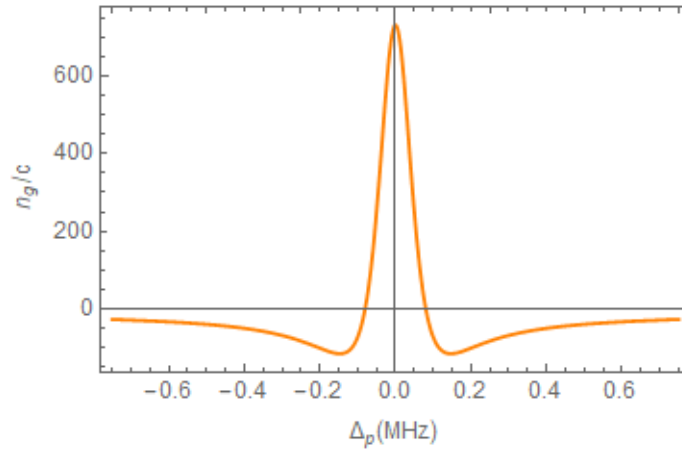


FIGURE 2.6: The group index n_g of probe light for $\Omega_p = 0.1\text{MHz}$, $\gamma_0 = \gamma_1 = 3.03\text{MHz}$, $N = 10^{20}\text{m}^{-3}$ and $\Omega_c = 1\text{MHz}$ in terms of the probe laser detuning.

Summary

In summary, this chapter has focused on the phenomenon of Electromagnetically Induced Transparency (EIT) within a single three-level Λ system driven by two incident fields. By performing electric susceptibility calculations, we can obtain the transparency window and

refractive index (group refractive index) in relation to EIT phenomena, thereby gaining valuable insights into the properties of light-matter interactions.

Chapter 3

Modelling a Dense Ensemble of 3-Level Λ systems

In this chapter, I give a brief review of a simple theoretical model in which the average behaviour of a quantum ensemble of 2-level atoms is effectively approximated by density matrix of a single particle with particular decoherence properties [29, 41]. Then, I apply this model to an ensemble of three-level Λ systems (3LAS). I start with an explanation of the generalized directional state basis to describe the behaviour of the atomic ensemble. After that, I present a model containing the decoherence terms involving effective spontaneous decay and dephasing rates, needed to model an ensemble of atomic systems with a single particle density matrix.

3.1 Maxwell–von Neumann Equations

In order to give a complete description of the atomic ensemble interacting with two driving light fields, one must necessarily solve self-consistently the coupled Maxwell's and the Lindblad-von-Neumann equations in three dimensions, where the radiation fields are governed by classical Maxwell's equations while the members of the ensemble are described quantum mechanically.

The temporal and spatial evolution of an electromagnetic wave through the optical

medium is determined by Maxwell's equations. Thus, according to Faraday's law and Ampere's law, we have

$$\begin{aligned}\vec{\nabla} \times \vec{E}(\vec{r}, t) &= -\mu_0 \dot{\vec{H}}(\vec{r}, t), \\ \vec{\nabla} \times \vec{H}(\vec{r}, t) &= \epsilon_0 \dot{\vec{E}}(\vec{r}, t) + \vec{J}(\vec{r}, t),\end{aligned}\quad (3.1)$$

where the dot stands for the time derivative, $\vec{J}(\vec{r}, t)$ is the free electric current density, $\vec{E}(\vec{r}, t)$ and $\vec{H}(\vec{r}, t)$ are the electric and magnetic fields, respectively, and μ_0 is the magnetic permeability of the free space.

In terms of the density matrix, the computation of the quantum dynamical system is made by using the Liouville-von Neumann equation

$$\dot{\rho} = -\frac{i}{\hbar} [H, \rho] - L(\rho), \quad (3.2)$$

where the dot stands for the time derivative, ρ is the density matrix operator that characterizes the statistical state of the system in the transformed frame, and H is the total Hamiltonian. In addition, $L(\rho)$ in the above evolution equation is the Lindblad superoperator defined by

$$L(\rho) = \sum_i \sum_j \frac{\gamma_{ij}}{2} \left(\sigma_{ij}^\dagger \sigma_{ij} \rho + \rho \sigma_{ij}^\dagger \sigma_{ij} - 2\sigma_{ij} \rho \sigma_{ij}^\dagger \right). \quad (3.3)$$

where σ_{ij} are the Lindblad operators, the superscript \dagger indicates Hermitian conjugation and γ_{ij} is the atom spontaneous emission rate from $|i\rangle$ to $|j\rangle$. For an emission transition from $|i\rangle$ to $|j\rangle$, the Lindblad operator is to be of the form

$$\sigma_{ij} = |j\rangle \langle i|. \quad (3.4)$$

In the presence of the electric fields applied, the macroscopic polarization describing the optical response of an atomic medium can contribute to the current density generation, $\vec{J}(\vec{r}, t)$. The components of the current density can be obtained from the macroscopic polarization by

$$\vec{J}(\vec{r}, t) = \frac{\partial}{\partial t} \vec{P}(\vec{r}, t), \quad (3.5)$$

where $\vec{P}(\vec{r}, t)$ is the macroscopic polarization given by

$$\begin{aligned}\vec{P}(\vec{r}, t) &= N \langle \vec{\mu} \rangle \\ &= N \text{Tr}(\rho \tilde{\mu}).\end{aligned}\tag{3.6}$$

In this equation, ρ is the density matrix, N is the atomic density and $\vec{\mu}$ is transition dipole moment which defined by the expression

$$\mu_i = -\frac{\partial H}{\partial E_i}, \quad i = x, y, z.\tag{3.7}$$

The above set of equations (3.1) and (3.2) with Hamiltonian can be solved numerically using finite difference time domain (FDTD) or pseudo-spectral time domain (PSTD) computation [29, 42, 43]. In these algorithms, the uniaxial perfectly-matched layer (PML) is implemented as the absorbing boundary condition (ABC) to truncate the computational domain [44]. Generally, in order to solve simultaneously the Maxwell and Lindblad-von Neumann equations, there are complex and voluminous calculations that take a considerable amount of time. Hence, a simple effective single particle model is constructed to examine the quantum dynamics of an atomic ensemble driven by electromagnetic fields.

3.2 Modeling an Ensemble of Atomic Systems with Directional Basis States

3.2.1 Two-Level Systems

Consider a simple system that is represented by a dense ensemble of two-level atoms consisting of ground $|g\rangle$ and excited $|e\rangle$ states with energy separation $\hbar\omega_{eg}$ (see Fig. 3.1) [29, 41]. This system is driven by an external linearly polarized electromagnetic plane-wave field with amplitude E_0 and frequency ω . The vector of incident light polarization is along the electric dipole direction of the individual particle. A noticeable effect of the ensemble of atoms is arising from the spontaneous emission of each atom, where these emissions can radiate electromagnetic fields with different polarization directions. Indeed, when a linear

polarized optical field is applied to the two-level medium, it is absorbed by an individual atom. The atom is therefore in its excited state, and hence one can expect that the light is emitted by the spontaneous decay process. The resulting light may be reabsorbed by a nearby ground-state atom. The spontaneous emission light may have multiple polarization directions, i.e., parallel and perpendicular to the initial incident polarization direction. These new polarization directions could interact with various orientations of the electric dipole moments of atoms in the ensemble [29].

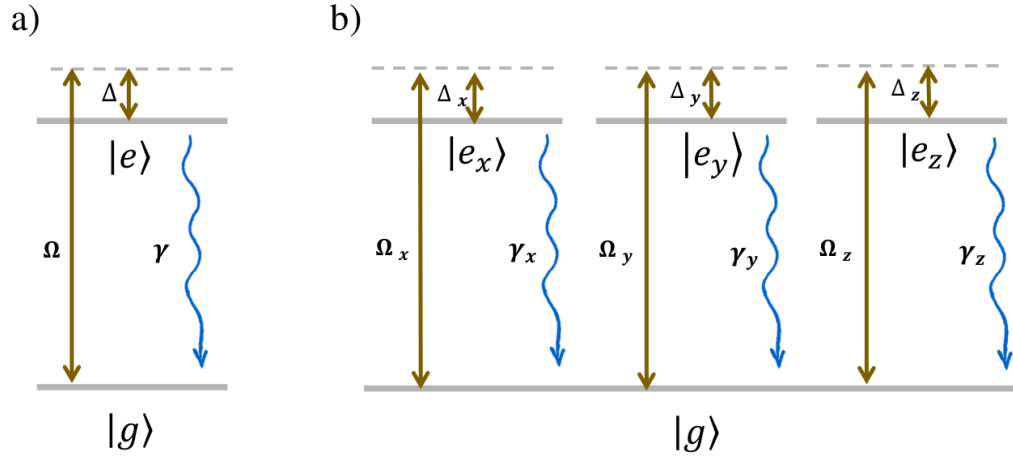


FIGURE 3.1: Schematic energy diagrams of an atomic system. a) The electric dipole moment of the two-level atom is oriented along the incident field polarization direction. b) The effective energy level structure of the two-level system that can be excited by the different field polarization components. Ω 's and Δ 's are the dipole-field interaction frequency and detuning, respectively. γ 's denote the spontaneous emission rates from the respective levels to the ground state [29].

In order to describe the quantum dynamics of an atomic ensemble driven by an external electromagnetic field, one has to take into account the excitation of atoms in directions other than the incident field polarization direction. This can be done by considering three excited directional states $|e_x\rangle$, $|e_y\rangle$ and $|e_z\rangle$ for atoms in the ensemble. A directional state basis was first proposed in [45] and later applied in Refs. [29, 41]. In this way, the atoms are represented by a four-level scheme with one ground state and three degenerate excited states. This is expressed diagrammatically in Fig. 3.1. It is clear that the excited states $|e_x\rangle$, $|e_y\rangle$ and $|e_z\rangle$ can couple to the ground state $|g\rangle$ by absorbing x , y or z -polarized light respectively.

3.2.2 Three-Level Λ Systems (3LAS)

To describe the time evolution of a quantum system that contains an ensemble of three-level atoms in the Λ configuration, we consider the five-level atom with three degenerate excited levels as the state of constituent elements of the ensemble. The energy structure of a five-level atom in a directional state basis is presented in Fig. 3.2. The two additional excited states are added to take into account the interatomic interactions between the atoms that produce excitations in other directions. Here, we assume the polarizations of two incident laser beams (probe and control) to be along the y -axis. Due to the spontaneous emission of an excited atom, the radiating atomic transition may be in the direction parallel to or perpendicular to the incident light polarization and which can be absorbed by another atom and thereby raise it into an excited state $|2y\rangle$, $|2x\rangle$ or $|2z\rangle$. The spontaneous emission and reabsorption events occur in different directions all over the ensemble. In Fig. 3.2, the decay rates of spontaneous emission from level $|2i\rangle$ to $|0\rangle$ and $|1\rangle$ are γ_{i0} and γ_{i1} , respectively, where $i = x, y$ or z .

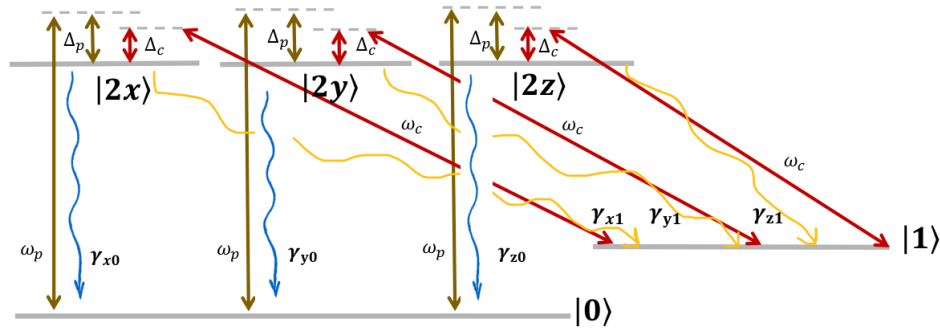


FIGURE 3.2: The effective energy level structure of the three-level Λ system that can be excited by the different field polarization components. ω_p and ω_c are the angular frequencies of the probe and control laser beams, respectively. Δ_p and Δ_c denote the detuning of the probe and the coupling fields with respect to their atomic transition energies.

3.3 Effective Single Particle Models of an Atomic Ensemble

3.3.1 Ensemble of Two-Level Atoms

The numerical solution to the Maxwell-Lindblad-von Neumann equations is associated with high computational complexity and long-time computation. Theoretically, the overall evolution of a driven atomic ensemble was shown to be quantitatively similar to that of a driven single-particle model in which the interatomic effects are described by decoherence terms. The decoherence rates can be calculated from the Forster resonance energy transfers process in biophysical modeling [46]. In the following, a review of the effective single-particle model of a two-level ensemble [29] is presented.

The nature of the atomic level structure of the single-atom model should be similar to the energy levels of constituent element of the ensemble. Thus, the single-atom model is comprised of a ground state $|g\rangle$ and three degenerate excited states $|e_x\rangle$, $|e_y\rangle$ and $|e_z\rangle$, where it can couple to the different polarization of electromagnetic field. The explicit Hamiltonian describing the effective single-atom driven by the electromagnetic wave, after the rotating wave approximation, takes the form

$$H_{ens} = -\frac{\hbar}{2} \begin{pmatrix} -2\Delta & \Omega_x & \Omega_y & \Omega_z \\ \Omega_x^* & 0 & 0 & 0 \\ \Omega_y^* & 0 & 0 & 0 \\ \Omega_z^* & 0 & 0 & 0 \end{pmatrix}, \quad (3.8)$$

where Δ shows the detuning between the optical frequency and the atomic transition, and the Rabi frequency of the electric field in three Cartesian directions is Ω_i , $i = x, y$ and z .

Following a manner that is similar to the case of the ensemble, consider that the external incident electric field is polarized along the y axis, E_y , hence the perpendicular field components, i.e. E_x and E_z , representing the scattered fields are much weak than the external incident field. These perpendicular fields arise due to spontaneous emission from the excited state of the atomic ensemble. Based on the field of dipole, one can roughly calculate the

perpendicular scattered field components as [29, 41]

$$E_{x,z} \sim E_y \frac{\mu}{er} \sin(\theta), \quad (3.9)$$

in which e is the elementary charge of an electron and μ is the atomic transition dipole moment. Moreover, we assume the presence of a cubic lattice and $r = \sqrt[3]{3\sqrt{8}/(4N\pi)}$ is the distance between nearest neighbors with being the number density N and θ is the angle between them and is equal $\theta = \pi/4$.

In the free-space situation, when an individual atom is excited in the states $|e_x\rangle$, $|e_y\rangle$ and $|e_z\rangle$, it can spontaneously radiate to the lower levels with rates γ_x , γ_y and γ_z . In contrast, in the ensemble, this radiation can be absorbed by another atom, giving rise to nontrivial atom-atom interactions. Thus, the radiation can be absorbed and re-emitted many times in an atomic ensemble. This process occurs for transition $|g\rangle \leftrightarrow |e_x, e_y, e_z\rangle$. Here, we assume that the effects of an ensemble are generally given in two ways: modifying the spontaneous decay rate and considering dephasing rate. For the single-particle model, one can calculate the effective spontaneous decay rate through the power radiated. And the dephasing rates can be predicted by models of the Forster-Resonance Energy Transfer process [46]. FRET occurs when a small light-emitting molecule (the “donor”) transfers its energy to a nearby molecule (the “acceptor”), typically occurring when the molecules are in close proximity to each other. In fact, the atom-atom interactions in the atomic ensemble are modeled by the dephasing terms based on the emission of a photon and the reabsorption of that photon by a neighbouring atom. Hence, we define δ_{ij} to be the dephasing rate for which photon is emitted from the state $|i\rangle$ of one atom and absorbed by another atom in the vicinity, which is then excited to the state $|j\rangle$. Typically, δ_{xx} , δ_{yy} and δ_{zz} are referred to as parallel dephasing rates, whereas δ_{xy} , δ_{xz} and δ_{yz} are referred to as perpendicular dephasing rates. The spontaneous decay and dephasing rates for the single-particle model are schematically displayed in Fig. 3.3. In the following, we give a derivation of the spontaneous emission and dephasing rates for the single-particle model.

Spontaneous Emission Rate

In order to obtain approximately the spontaneous emission rates for an effective single particle model, we use the radiated power of an atom determined by the Larmor formula.

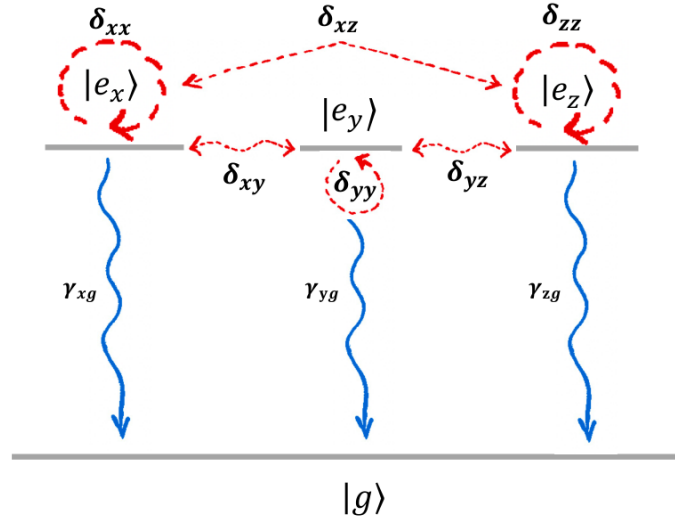


FIGURE 3.3: A sketch of the transition structure in the effective single-particle model of the driven ensemble of atoms. The blue and red dashed curves correspond to the spontaneous emission and dephasing due to interatomic energy transfer [29].

By comparing the ratio of the power emitted by an atom in an ensemble and free space, one can estimate the spontaneous emission rate from the excited state to the lower state in an ensemble. This ratio is given as

$$\frac{\gamma'_{ij}}{\gamma_{ij}} = \frac{P'}{P} = \frac{\text{Re}(\tilde{\mathbf{j}}_{ij}^* \cdot \tilde{\mathbf{E}}_{\text{mean}})}{\text{Re}(\tilde{\mathbf{j}}_{ij}^* \cdot \tilde{\mathbf{E}}_{\text{inc}})}, \quad (3.10)$$

where γ'_{ij} (P') and γ_{ij} (P) are the atom spontaneous emission rates (power emitted) from $|i\rangle$ to $|j\rangle$ in the ensemble and free space, respectively, \vec{j}_{ij} is the free current of the transition $|i\rangle \leftrightarrow |j\rangle$ that relates to the atomic electric dipole moment $\vec{\mu}_{ij}$ as $\vec{j}_{ij} = -i\omega\vec{\mu}_{ij}$. Consequently, the above equation can be written in terms of the dipole moment as follows

$$\frac{\gamma'_{ij}}{\gamma_{ij}} = \frac{\text{Im}(\tilde{\mu}_{ij}^* \cdot \tilde{\mathbf{E}}_{\text{mean}})}{\text{Im}(\tilde{\mu}_{ij}^* \cdot \tilde{\mathbf{E}}_{\text{inc}})}. \quad (3.11)$$

Since the mean field is the sum of the incident field and the scattered field, $\vec{E}_{\text{mean}} = \vec{E}_{\text{inc}} + \vec{E}_{\text{ext}}$, we have

$$\frac{\gamma'_{ij}}{\gamma_{ij}} = 1 + \frac{\text{Im}(\tilde{\mu}_{ij}^* \cdot \tilde{\mathbf{E}}_{\text{ext}})}{\text{Im}(\tilde{\mu}_{ij}^* \cdot \tilde{\mathbf{E}}_{\text{inc}})}. \quad (3.12)$$

In the case of single particle model, there is no scattered field amplitude, $\vec{E}_{\text{ext}} = 0$, and thus the spontaneous emission rates γ'_{ij} are equal to γ_{ij} . The spontaneous emission rates

do not change for the single particle model.

Dephasing Rate

The dephasing rate, δ_{ij} , is interpreted as the rate of energy transfer between atomic transitions and is determined based on the Forster-Resonance Energy Transfer mechanism [29, 46]. The magnitude of the dephasing rate can be calculated from the ratio of the power transferred from the state $|i\rangle$ into the state $|j\rangle$, $P_{i\rightarrow j}$, to the power emitted by an atom in free space, expressed as

$$\frac{\delta_{i\rightarrow j}}{\gamma_{ik}} = \frac{P_{i\rightarrow j}}{P_{ik}}, \quad (3.13)$$

where $\delta_{i\rightarrow j}$ is the dephasing rate from i (donor) to j (acceptor) and γ_{ik} is the spontaneous emission rates from the state $|i\rangle$ to the lower state $|k\rangle$ with the power emitted P_{ik} in free space. The power transferred $P_{i\rightarrow j}$ from donor to acceptor is

$$P_{i\rightarrow j} = -\frac{1}{2} \text{Re}(\tilde{j}_j^*(\tilde{r}_j) \cdot \tilde{E}_i(\tilde{r}_j)), \quad (3.14)$$

with the current density of the acceptor \vec{j}_j and the electric field $\vec{E}_i(\vec{r}_j)$ of the donor at the acceptor position.

Regarding to the electric field of a point dipole

$$\vec{E}_i(\vec{r}) = \frac{1}{4\pi\epsilon_0} \left(\frac{3(\vec{\mu}_i \cdot \hat{r})\hat{r} - \vec{\mu}_i}{r^3} \right), \quad (3.15)$$

with the dipole moment of transition $\vec{\mu}_i$ and distance apart of atoms $1/r^3 = 1/8 \times 4\pi N/3$, we have

$$\vec{E}_i(\vec{r}) = \frac{N}{24\epsilon_0} |\mu_i| (3(\hat{\mu}_i \cdot \hat{r})\hat{r} - \hat{\mu}_i). \quad (3.16)$$

Using the above electric field and the current density $\vec{j}_i = -i\omega\vec{\mu}_i$, the power transferred $P_{i\rightarrow j}$ becomes

$$P_{i\rightarrow j} = \frac{1}{2} \omega \vec{\mu}_j \cdot \left(\frac{N}{24\epsilon_0} |\mu_i| (3(\hat{\mu}_i \cdot \hat{r}_j)\hat{r}_j - \hat{\mu}_i) \right). \quad (3.17)$$

Assuming that the amplitudes of the dipole moments for each transition are equal, $|\mu_{i,j}| =$

$|\mu|$, $P_{i \rightarrow j}$ takes the form

$$\begin{aligned} P_{i \rightarrow j} &= \frac{N\omega}{48\epsilon_0} |\mu|^2 (3(\hat{\mu}_i \cdot \hat{r}_j)(\hat{\mu}_j \cdot \hat{r}_j) - (\hat{\mu}_j \cdot \hat{\mu}_i)) \\ &= \frac{N\omega}{48\epsilon_0} |\mu|^2 (3(\hat{\mu}_i \cdot \hat{r}_j) - (\hat{\mu}_j \cdot \hat{\mu}_i)). \end{aligned} \quad (3.18)$$

In this way, we have estimated dephasing and emission based on dipolar fields from other atoms self consistently. With the power transferred $P_{i \rightarrow j}$ at hand, one can obtain the dephasing rate as

$$\frac{\delta_{i \rightarrow j}}{\gamma_{ik}} = \frac{P_{i \rightarrow j}}{P_{ik}} = \frac{N\omega |\mu|^2 (3(\hat{\mu}_i \cdot \hat{r}_j) - (\hat{\mu}_j \cdot \hat{\mu}_i)) / (48\epsilon_0)}{\mu_0 \omega^4 |\mu|^2 / (12\pi c)}, \quad (3.19)$$

where we have used $P_{ik} = \mu_0 \omega^4 |\mu|^2 / (12\pi c)$ for the power emitted in free space. After simplifying, this reduces to

$$\frac{\delta_{i \rightarrow j}}{\gamma_{ik}} = \frac{N\pi c^3}{4\omega_{ik}^3} (3(\hat{\mu}_i \cdot \hat{r}_j) - \hat{\mu}_j \cdot \hat{\mu}_i). \quad (3.20)$$

In order to take into account the fraction of atoms undergoing the transition in the ensemble, we add a factor of $\sqrt{\rho_{ii}\rho_{kk}}\sqrt{\rho_{jj}\rho_{kk}}$ to this equation. We find

$$\frac{\delta_{i \rightarrow j}}{\gamma_{ik}} = \frac{N\pi c^3}{4\omega_{ik}^3} (3(\hat{\mu}_i \cdot \hat{r}_j) - \hat{\mu}_j \cdot \hat{\mu}_i) \sqrt{\rho_{ii}\rho_{kk}}\sqrt{\rho_{jj}\rho_{kk}}. \quad (3.21)$$

As one can see from above equation, for the parallel dephasing rates, we have

$$\frac{\delta_{i \rightarrow i}}{\gamma_{ik}} = \frac{N\pi c^3}{2\omega_{ik}^3} (\sqrt{\rho_{ii}\rho_{kk}}\sqrt{\rho_{ii}\rho_{kk}}), \quad (3.22)$$

where $\delta_{i \rightarrow i}$ is the rate of energy transfer from state i in one atom to i in another atom. And finally, for the perpendicular dephasing rates, we have

$$\frac{\delta_{i \rightarrow j}}{\gamma_{ik}} = \frac{3N\pi c^3}{16\sqrt{2}\omega_{ik}^3} (\sqrt{\rho_{ii}\rho_{kk}}\sqrt{\rho_{jj}\rho_{kk}}), \quad (3.23)$$

where we have multiplied the equation (3.21) by a factor $1/\sqrt{8}$ due to the nearest diagonal neighbour, instead of the nearest neighbour distribution. Note that the dephasing rates are functions of time through their dependence on the density matrix element. I will then apply this methodology to design a single particle model of an ensemble of 3L Λ systems.

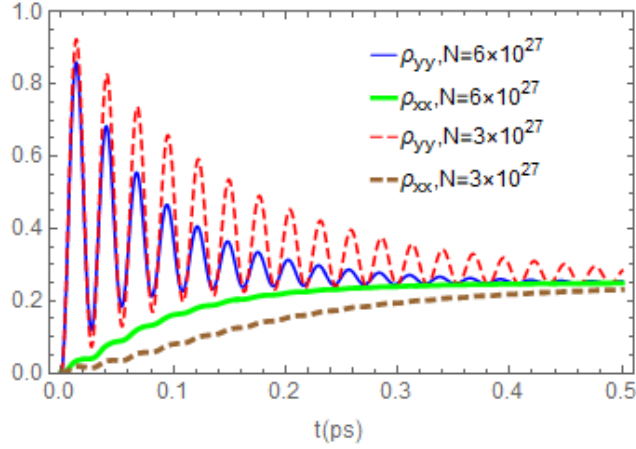


FIGURE 3.4: Excited state populations of single particle model as a function of time for two values of number density of atoms in the ensemble. The amplitude of the driving electric field E is $1.5 \times 10^9 \text{V/m}$. Here we have set $\Delta = 0$ [29].

Given the spontaneous decay and dephasing rates, one can construct the Lindblad superoperator. One can then solve the Lindblad-von Neumann equation by setting the initial conditions $\rho_{gg} = 1$, $\rho_{xx} = 0$, $\rho_{yy} = 0$ and $\rho_{zz} = 0$. The temporal evolution of excited-state populations are presented in Fig. 3.4. Here, the spontaneous emission rates are estimated using Fermi's golden rule equation [46]. Looking at figure 3.4, one can clearly see the influence of the number density of atoms on the dynamics of excited state populations.

3.3.2 Ensemble of 3-Level Λ Systems

Here, we generalize the previous procedure to the case of a five-level atomic system driven by two laser fields, where the electromagnetically induced transparency process can be created.

In this modeling technique, the atomic-level structure for the single-particle density matrix is the same as that taken for an atom in the ensemble. So, it has two closely ground states $|0\rangle$ and $|1\rangle$ and three degenerate excited directional states $|2x\rangle$, $|2y\rangle$ and $|2z\rangle$ (Fig. 3.5).

The total Hamiltonian of this five-level atom interacting with the electromagnetic field can be written as

$$H = H_0 + H_1, \quad (3.24)$$

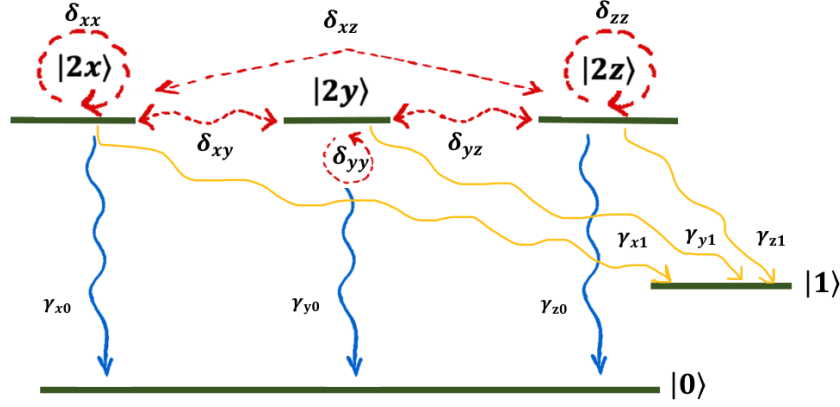


FIGURE 3.5: A sketch of the transition structure in the effective single-particle model of the driven ensemble of atoms. The blue (orange) and red dashed curves correspond to the spontaneous emission and dephasing due to interatomic energy transfer.

where H_0 is the bare Hamiltonian of the atom which is represented in matrix form as

$$H_0 = \begin{pmatrix} \hbar\omega_0 & 0 & 0 & 0 & 0 \\ 0 & \hbar\omega_1 & 0 & 0 & 0 \\ 0 & 0 & \hbar\omega_2 & 0 & 0 \\ 0 & 0 & 0 & \hbar\omega_2 & 0 \\ 0 & 0 & 0 & 0 & \hbar\omega_2 \end{pmatrix}, \quad (3.25)$$

in which $\hbar\omega_0$, $\hbar\omega_1$ and $\hbar\omega_2$ are the eigenvalues of H_0 . In Eq. (3.24), H_1 is the interaction Hamiltonian given by

$$H_1 = -\vec{\mu} \cdot \vec{E}, \quad (3.26)$$

\vec{E} is the total electric field which is a sum of the incident and local electric fields

$$\vec{E} = \vec{E}_{inc} + \vec{E}_{local}. \quad (3.27)$$

In the above, the local electric field is caused by the spontaneous decay of excited atoms in the ensemble. Since these are two applied fields (the probe and control), we can write the total electric field \vec{E} experienced within the ensemble as

$$\begin{aligned} \vec{E} = & (\hat{x}E_{px} + \hat{y}E_{py} + \hat{z}E_{pz}) \cos(\omega_p t) \\ & + (\hat{x}E_{cx} + \hat{y}E_{cy} + \hat{z}E_{cz}) \cos(\omega_c t), \end{aligned} \quad (3.28)$$

where we consider the dipole approximation. A weak probe field with angular frequency ω_p , amplitude E_{py} and unit polarization vector \hat{y} couples the dipole allowed transition $|0\rangle \leftrightarrow |2y\rangle$; a strong coupling field with angular frequency ω_c , amplitude E_{cy} and unit polarization vector \hat{y} couples the dipole allowed transition $|1\rangle \leftrightarrow |2y\rangle$. Note that, two electric fields with amplitudes E_{px} and E_{pz} (E_{cx} and E_{cz}) and unit polarization vectors \hat{x} and \hat{z} (\hat{x} and \hat{z}) generated by spontaneous emission drive, respectively, the transitions $|0\rangle \leftrightarrow |2x\rangle$ and $|0\rangle \leftrightarrow |2z\rangle$ ($|1\rangle \leftrightarrow |2x\rangle$ and $|1\rangle \leftrightarrow |2z\rangle$). These electric fields arise from the spontaneous emission transitions perpendicular to the polarization vectors of incident field components, i.e. probe and control fields.

In the above equation (3.26), $\vec{\mu}$ is the atomic electric dipole moment operator given by

$$\begin{aligned} \vec{\mu} = \hat{x} & \begin{pmatrix} 0 & 0 & 1 & 0 & 0 \\ 0 & 0 & 0 & 0 & 0 \\ 1 & 0 & 0 & 0 & 0 \\ 0 & 0 & 0 & 0 & 0 \\ 0 & 0 & 0 & 0 & 0 \end{pmatrix} \mu_{02x} + \hat{y} \begin{pmatrix} 0 & 0 & 0 & 1 & 0 \\ 0 & 0 & 0 & 0 & 0 \\ 0 & 0 & 0 & 0 & 0 \\ 1 & 0 & 0 & 0 & 0 \\ 0 & 0 & 0 & 0 & 0 \end{pmatrix} \mu_{02y} + \hat{z} \begin{pmatrix} 0 & 0 & 0 & 0 & 1 \\ 0 & 0 & 0 & 0 & 0 \\ 0 & 0 & 0 & 0 & 0 \\ 0 & 0 & 0 & 0 & 0 \\ 1 & 0 & 0 & 0 & 0 \end{pmatrix} \mu_{02z} \\ + \hat{x} & \begin{pmatrix} 0 & 0 & 0 & 0 & 0 \\ 0 & 0 & 1 & 0 & 0 \\ 0 & 1 & 0 & 0 & 0 \\ 0 & 0 & 0 & 0 & 0 \\ 0 & 0 & 0 & 0 & 0 \end{pmatrix} \mu_{12x} + \hat{y} \begin{pmatrix} 0 & 0 & 0 & 0 & 0 \\ 0 & 0 & 0 & 1 & 0 \\ 0 & 0 & 0 & 0 & 0 \\ 0 & 1 & 0 & 0 & 0 \\ 0 & 0 & 0 & 0 & 0 \end{pmatrix} \mu_{12y} + \hat{z} \begin{pmatrix} 0 & 0 & 0 & 0 & 0 \\ 0 & 0 & 0 & 0 & 1 \\ 0 & 0 & 0 & 0 & 0 \\ 0 & 0 & 0 & 0 & 0 \\ 0 & 1 & 0 & 0 & 0 \end{pmatrix} \mu_{12z}, \quad (3.29) \end{aligned}$$

According to the above description, the matrix form of the interacting Hamiltonian is given by

$$H_1 = -\hbar \begin{pmatrix} 0 & 0 & \Omega_{px} \cos(\omega_p t) & \Omega_{py} \cos(\omega_p t) & \Omega_{pz} \cos(\omega_p t) \\ 0 & 0 & \Omega_{cx} \cos(\omega_c t) & \Omega_{cy} \cos(\omega_c t) & \Omega_{cz} \cos(\omega_c t) \\ \Omega_{px} \cos(\omega_p t) & \Omega_{cx} \cos(\omega_c t) & 0 & 0 & 0 \\ \Omega_{py} \cos(\omega_p t) & \Omega_{cy} \cos(\omega_c t) & 0 & 0 & 0 \\ \Omega_{pz} \cos(\omega_p t) & \Omega_{cz} \cos(\omega_c t) & 0 & 0 & 0 \end{pmatrix}, \quad (3.30)$$

where the real Rabi frequencies are defined as

$$\begin{aligned}\Omega_{px} &= \frac{\mu_{02x}E_{px}}{\hbar}, & \Omega_{py} &= \frac{\mu_{02y}E_{py}}{\hbar}, & \Omega_{pz} &= \frac{\mu_{02z}E_{pz}}{\hbar}, \\ \Omega_{cx} &= \frac{\mu_{12x}E_{cx}}{\hbar}, & \Omega_{cy} &= \frac{\mu_{12y}E_{cy}}{\hbar}, & \Omega_{cz} &= \frac{\mu_{12z}E_{cz}}{\hbar}.\end{aligned}\quad (3.31)$$

In the following, the cosine functions in H_1 Eq. (3.30) are conveniently represented in terms of the exponential form using Euler's formula.

Now, by specifying the spontaneous emission and dephasing rates, one can find the dynamics of the effective single-particle in the presence of two external driving fields by means of the time evolution of the density matrix given by the Liouville-von Neumann equation

$$\dot{\rho} = -\frac{i}{\hbar} [H, \rho] - L(\rho), \quad (3.32)$$

with the total Hamiltonian H , and the Lindblad superoperator $L(\rho)$ expressed in terms of the spontaneous emission and dephasing rates

$$\begin{aligned}L(\rho) &= \sum_{i=2x,2y,2z} \sum_{j=0,1} \frac{\gamma_{ij}}{2} \left(\sigma_{ij}^\dagger \sigma_{ij} \rho + \rho \sigma_{ij}^\dagger \sigma_{ij} - 2\sigma_{ij} \rho \sigma_{ij}^\dagger \right) \\ &+ \sum_{i=2x,2y,2z} \sum_{j=2x,2y,2z} \frac{\delta_{ij}}{2} \left(\sigma_{ij}^\dagger \sigma_{ij} \rho + \rho \sigma_{ij}^\dagger \sigma_{ij} - 2\sigma_{ij} \rho \sigma_{ij}^\dagger \right).\end{aligned}\quad (3.33)$$

For an emission transition from $|i\rangle$ to $|j\rangle$, the Lindblad operator is to be of the form

$$\sigma_{ij} = |j\rangle \langle i|. \quad (3.34)$$

In particular, for instance, the Lindblad operator for the spontaneous decay from $|2x\rangle$ to $|0\rangle$ has the following matrix representation

$$\sigma_{2x0} = \begin{pmatrix} 0 & 0 & 1 & 0 & 0 \\ 0 & 0 & 0 & 0 & 0 \\ 0 & 0 & 0 & 0 & 0 \\ 0 & 0 & 0 & 0 & 0 \\ 0 & 0 & 0 & 0 & 0 \end{pmatrix}. \quad (3.35)$$

Now, by introducing the unitary matrix transformation of

$$U = \begin{pmatrix} e^{-i(\omega_p+\omega_2)t} & 0 & 0 & 0 & 0 \\ 0 & e^{-i(\omega_c+\omega_2)t} & 0 & 0 & 0 \\ 0 & 0 & e^{-i\omega_2t} & 0 & 0 \\ 0 & 0 & 0 & e^{-i\omega_2t} & 0 \\ 0 & 0 & 0 & 0 & e^{-i\omega_2t} \end{pmatrix}, \quad (3.36)$$

we obtain the transformed interaction Hamiltonian H_1 as follows

$$UH_1U^\dagger = -\hbar \begin{pmatrix} 0 & 0 & \frac{\Omega_{px}}{2}\mathcal{A} & \frac{\Omega_{py}}{2}\mathcal{A} & \frac{\Omega_{pz}}{2}\mathcal{A} \\ 0 & 0 & \frac{\Omega_{cx}}{2}\mathcal{B} & \frac{\Omega_{cy}}{2}\mathcal{B} & \frac{\Omega_{cz}}{2}\mathcal{B} \\ \frac{\Omega_{px}}{2}\mathcal{A}^* & \frac{\Omega_{cx}}{2}\mathcal{B}^* & 0 & 0 & 0 \\ \frac{\Omega_{py}}{2}\mathcal{A}^* & \frac{\Omega_{cy}}{2}\mathcal{B}^* & 0 & 0 & 0 \\ \frac{\Omega_{pz}}{2}\mathcal{A}^* & \frac{\Omega_{cz}}{2}\mathcal{B}^* & 0 & 0 & 0 \end{pmatrix}, \quad (3.37)$$

where the superscript asterisk denotes taking the complex conjugate and the parameters are

$$\mathcal{A} = 1 + e^{2i\omega_p t}, \quad \mathcal{B} = 1 + e^{2i\omega_c t}. \quad (3.38)$$

By adopting the rotating wave approximation and neglecting the fast-oscillating terms in Eq. (3.37), we arrive at

$$UH_1U^\dagger = -\frac{\hbar}{2} \begin{pmatrix} 0 & 0 & \Omega_{px} & \Omega_{py} & \Omega_{pz} \\ 0 & 0 & \Omega_{cx} & \Omega_{cy} & \Omega_{cz} \\ \Omega_{px} & \Omega_{cx} & 0 & 0 & 0 \\ \Omega_{py} & \Omega_{cy} & 0 & 0 & 0 \\ \Omega_{pz} & \Omega_{cz} & 0 & 0 & 0 \end{pmatrix}. \quad (3.39)$$

Finally, the total Hamiltonian in the transformed frame is

$$H_{RWA} = -\frac{\hbar}{2} \begin{pmatrix} -2\Delta_p & 0 & \Omega_{px} & \Omega_{py} & \Omega_{pz} \\ 0 & -2\Delta_c & \Omega_{cx} & \Omega_{cy} & \Omega_{cz} \\ \Omega_{px} & \Omega_{cx} & 0 & 0 & 0 \\ \Omega_{py} & \Omega_{cy} & 0 & 0 & 0 \\ \Omega_{pz} & \Omega_{cz} & 0 & 0 & 0 \end{pmatrix}, \quad (3.40)$$

where $\Delta_p = \omega_p - \omega_2 + \omega_0$ and $\Delta_c = \omega_c - \omega_2 + \omega_1$ are the detunings of the control and probe field frequencies from atomic resonance frequencies. More details are provided in Appendix A. The above Hamiltonian is used to describe the interaction of an atomic ensemble with the incident fields.

So, the Lindblad-von Neumann equation becomes

$$\dot{\rho} = -\frac{i}{\hbar} [H_{RWA}, \rho] - L(\rho), \quad (3.41)$$

with the Hamiltonian H_{RWA} (A.7) and the Lindblad superoperator $L(\rho)$ expressed in terms of the spontaneous emission and dephasing rates

$$\begin{aligned} L(\rho) &= \sum_{i=2x,2y,2z} \sum_{j=0,1} \frac{\gamma_{ij}}{2} \left(\sigma_{ij}^\dagger \sigma_{ij} \rho + \rho \sigma_{ij}^\dagger \sigma_{ij} - 2\sigma_{ij} \rho \sigma_{ij}^\dagger \right) \\ &+ \sum_{i=2x,2y,2z} \sum_{j=2x,2y,2z} \frac{\delta_{ij}}{2} \left(\sigma_{ij}^\dagger \sigma_{ij} \rho + \rho \sigma_{ij}^\dagger \sigma_{ij} - 2\sigma_{ij} \rho \sigma_{ij}^\dagger \right). \end{aligned} \quad (3.42)$$

The above Liouville–von-Neumann equations (3.41) comprise 15 independent first-order coupled differential equations for the elements of the density matrix.

Summary

In summary, in this chapter, a simple theoretical model that effectively approximates the average behavior of a quantum ensemble of three-level atoms is described using the density matrix of a single particle with specific decoherence properties. To do so, I modelled 3LAS with a multi-directional excited state. Subsequently, I applied a model that includes decoherence terms related to effective spontaneous decay and dephasing rates. These terms

are essential for accurately modeling an ensemble of atomic systems with a single particle density matrix. By using this methodology, I investigate the EIT effect in the next chapter.

Chapter 4

Modelling EIT in an Atomic Ensemble

In this chapter, I numerically model EIT in an ensemble of 3LAS and examine the effect of the number density of atoms on the bandwidth of the EIT window and the group velocity. First, I model the ensemble using a single particle density matrix (3.3.2) and calculate transparency window and group velocity for a probe field (2.2). Then, I investigate the propagation of a probe Gaussian pulse in an atomic medium of 3LAS by solving the coupled Maxwell and Liouville-von Neumann equations in the limit that the variation in the electric field is very slow over space and time. I examine the dependence of EIT on the number density of the ensemble.

4.1 EIT in an Atomic Ensemble: Single Particle Model

By using the single particle model of the ensemble of 3LAS as described previously in chapter 3, and also using the system parameters from the inputs for a ^{87}Rb experiment [34], I solved numerically Liouville-von Neumann equations simultaneously by assuming the initial condition

$$\rho_{00} = 1, \quad \rho_{11} = 0, \quad \rho_{2x2x} = 0, \quad \rho_{2y2y} = 0, \quad \rho_{2z2z} = 0. \quad (4.1)$$

I obtained the solutions to equation 3.41 by using the NDSolve function of Wolfram Mathematica.

Linear Susceptibility of the Ensemble

I calculated the probe susceptibility from the numerical steady-state solution of the Liouville-von Neumann equation. The electric susceptibility in the linear response of the probe field is calculated from the density matrix. The induced linear polarization of the atomic medium driven by a weak probe field at the probe frequency ω_p is

$$P_y = \frac{1}{2}\epsilon_0 E_{py} [\chi_{py}(\omega_p) e^{-i\omega_p t} + \chi_{py}(\omega_p)^* e^{i\omega_p t}]. \quad (4.2)$$

Comparing this formula with the equation (2.19) in chapter 2, one difference is that instead of using E_p , we use E_{py} in an ensemble. In addition, the polarization in the y direction is also achieved by calculating a quantum average of the y component of dipole moment at the probe frequency ω_p . This yields

$$\begin{aligned} P_y &= N \text{Tr}(\rho \hat{\mu}_{02y}) \\ &= N \mu_{02y} (\rho_{2y0} e^{-i\omega_p t} + \rho_{02y} e^{i\omega_p t}). \end{aligned} \quad (4.3)$$

By matching the coefficient of $e^{-i\omega_p t}$ in equations (4.2) and (4.3), the linear probe susceptibility is derived as

$$\chi_{py} = \frac{2N \mu_{02y}^2}{\epsilon_0 \hbar \Omega_{py}} \rho_{2y0}, \quad (4.4)$$

where the Rabi frequency, $\Omega_{py} = E_{py} \mu_{02y} / \hbar$.

I consider a system of alkali ^{87}Rb atoms, where I set the three levels $|0\rangle = |5S_{1/2}, F = 1\rangle$, $|1\rangle = |5S_{1/2}, F = 2\rangle$ and $|2\rangle = |5P_{3/2}, F = 2\rangle$ [34]. The parameters I used are $\Omega_{py} = 0.1\text{MHz}$, $\Omega_{cy} = 1\text{MHz}$, $N = 10^{24} m^{-3}$, $\gamma_{2x0} = \gamma_{2y0} = \gamma_{2z0} = \gamma_0 = 3.03\text{MHz}$ and $\gamma_{2x1} = \gamma_{2y1} = \gamma_{2z1} = \gamma_1 = 3.03\text{MHz}$. Here, I assume $\gamma_{2x0} = \gamma_{2y0} = \gamma_{2z0} = \gamma_0$ and $\gamma_{2x1} = \gamma_{2y1} = \gamma_{2z1} = \gamma_1$ for calculations.

In order to compare the behavior of electric susceptibility of the 3LAS and an ensemble of 3LAS, the imaginary and real components of χ_{py} with Δ_p are depicted in Figs. 4.1 and 4.2. From Fig. 4.1, it is seen that the transparency window for an ensemble is slightly

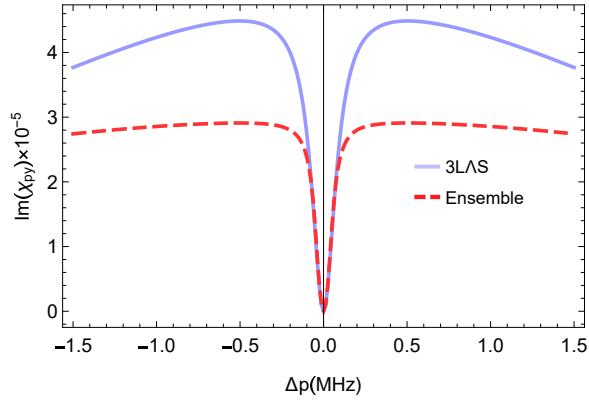


FIGURE 4.1: The imaginary part of the susceptibility χ_{py} for the single 3LAS and an ensemble of 3LAS with parameters $\Omega_{py} = 0.1\text{MHz}$, $\Omega_{cy} = 1\text{MHz}$, $\gamma_0 = \gamma_1 = 3.03\text{MHz}$, $N = 10^{24}m^{-3}$ and $\Delta_c = 0$ in terms of the probe laser detuning. The dip in $Im_{\chi_{py}}$ shows the narrowing of the EIT window.

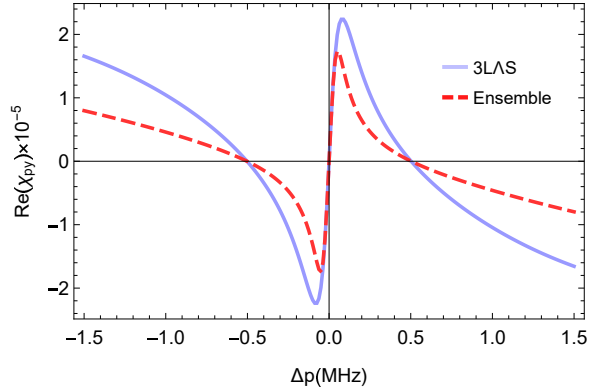


FIGURE 4.2: The real part of the susceptibility χ_{py} for the single 3LAS and an ensemble of 3LAS with parameters $\Omega_{py} = 0.1\text{MHz}$, $\Omega_{cy} = 1\text{MHz}$, $\gamma_0 = \gamma_1 = 3.03\text{MHz}$, $N = 10^{24}m^{-3}$ and $\Delta_c = 0$ in terms of the probe laser detuning.

narrowed compared with the case of a single atom, and the Gaussian profile becomes flatter. According to Fig. 4.2, one can see that the peaks become weaker and narrower for an ensemble around the resonance transition and also positive slope of the susceptibility is the same for both of them. The achievable frequency range (bandwidth) for slow light has reduced, leading to a decrease in the full-width at half-maximum (FWHM).

The refractive index for the probe field in the medium $n(\omega_{py})$ is obtained from the real part of susceptibility (χ_{py}) via the following equation

$$n(\omega_{py}) = 1 + \text{Re}(\chi_{py})/2. \quad (4.5)$$

Figure 4.3 illustrates the calculated group refractive index of the probe light for both the

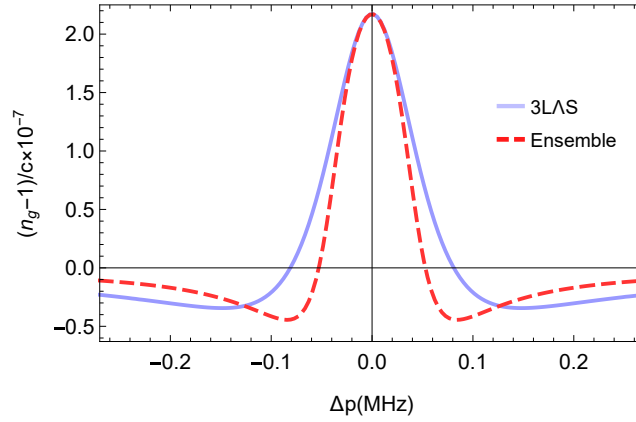


FIGURE 4.3: The group refractive index of probe light for the 3LAS and an ensemble of 3LAS as a function of Δ_p with $\Omega_{py} = 0.1\text{MHz}$, $\Omega_{cy} = 1\text{MHz}$, $\gamma_0 = \gamma_1 = 3.03\text{MHz}$, $\Delta_c = 0$.

3LAS and an ensemble of 3LAS as a function of Δ_p . Notably, in this figure, the maximum value of the refractive group index is observed for both cases at $\Delta_p = 0$, corresponding to the lowest value of the group velocity.

All three graphs (Figs. 4.1, 4.2, and 4.3), share a common observation that the transparency window and the slow light window are narrower. Consequently, achieving slow light requires longer and longer pulses in an ensemble. It's important to note that the parameters have been fixed for these graphs, specifically $\Omega_p = 0.1\text{MHz}$, $\Omega_c = 1\text{MHz}$, $\gamma_0 = \gamma_1 = 3.03\text{MHz}$, $\Delta_c = 0$, and $N = 10^{24}\text{m}^{-3}$.

4.1.1 Effect of Number Density

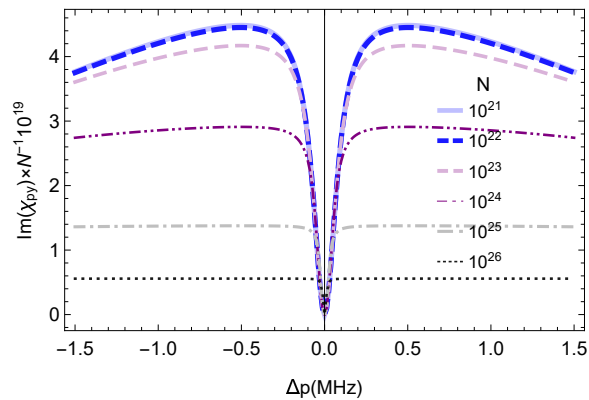


FIGURE 4.4: The imaginary part of the susceptibility as a function of probe laser detuning for $\Omega_{py} = 0.1\text{MHz}$, $\Omega_{cy} = 1\text{MHz}$, $\gamma_0 = \gamma_1 = 3.03\text{MHz}$, $\Delta_c = 0$ and various values of the number density N .

In the single particle model of the ensemble, the dephasing rates are number density dependant. Hence, to examine the effect of number density on the electric susceptibility, we plot the imaginary part of electric susceptibility as a function of Δ_p for different values of the number density in Fig 4.4. In this case, at number densities of $N = 10^{21}m^{-3}$ and $N = 10^{22}m^{-3}$, both the 3LAS and an ensemble of 3LAS exhibit agreement with each other. However, as the number density increases further, a notable decrease in the EIT window is observed. This finding indicates a strong dependence on the density of the ensemble, revealing how collective effects play a crucial role in shaping the EIT behavior in the system.

To further clarify the effect of number density on the transparency window width, the full-width at half-maximum (FWHM) of the transparency window is depicted in Fig. 4.5.

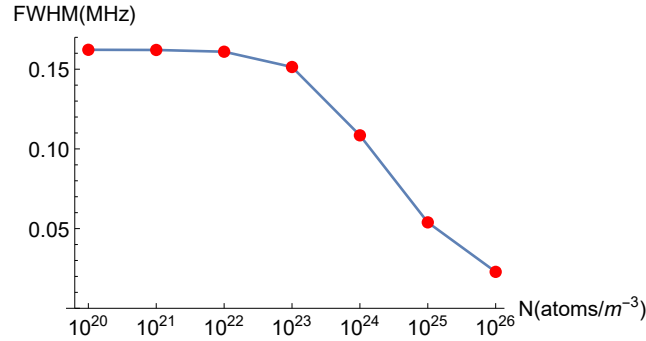


FIGURE 4.5: FWHM of the imaginary part of the susceptibility as a function of number density N for the same parameters as in Fig. 4.4.

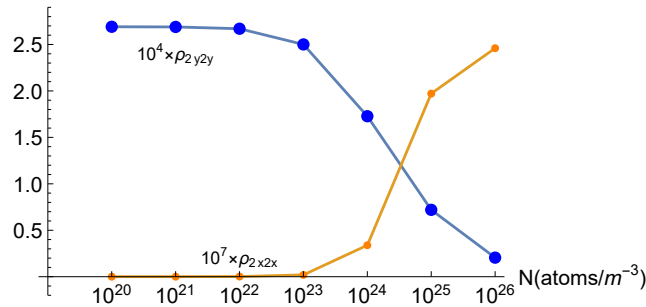


FIGURE 4.6: Populations ρ_{2x2x} and ρ_{2y2y} in the x and y directional excited states as a function of number density N for the same parameters as in Fig. 4.4. The y direction is the polarization of the incident field.

We can see that at lower N values, the behavior of the ensemble closely resembles that of a single atom, but as N increases, the change becomes non-linear. It is clearly seen that with increasing number density N , the behaviour of an ensemble appears from around $N = 10^{23}m^{-3}$. For the sake of clarity, the excited state populations in the x and y directions

are sketched in Fig. 4.6. As the number density approaches $N = 10^{23}m^{-3}$, the population is leaking in other directions compared to initial states, and that correlates to the drop in FWHM in Fig. 4.5. It is important to highlight that as the number density increases to very large densities, the limitations of this model become apparent, as we have not accounted for various other possible interactions and couplings.

The calculated group refractive index of probe light for an ensemble as a function of Δ_p for different values of the number density N is shown in Fig. 4.7 with the parameters $\Omega_{py} = 0.1\text{MHz}$, $\Omega_{cy} = 1\text{MHz}$, $\gamma_0 = \gamma_1 = 3.03\text{MHz}$. As the number density increases, there is a noticeable and rapid change in the refractive index around the transparency window.

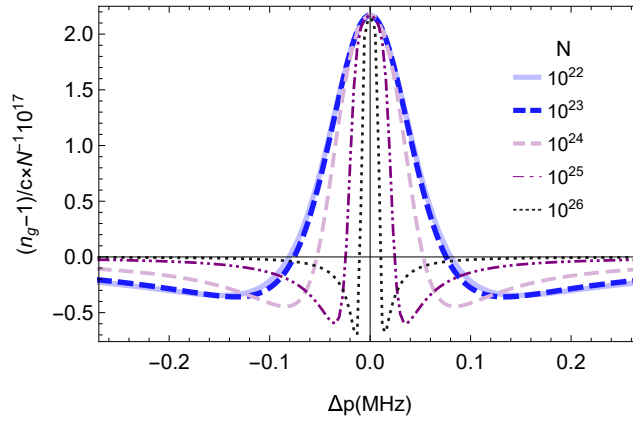


FIGURE 4.7: The group refractive index of probe light as a function of probe laser detuning for $\Omega_{py} = 0.1\text{MHz}$, $\Omega_{cy} = 1\text{MHz}$, $\gamma_0 = \gamma_1 = 3.03\text{MHz}$, $\Delta_c = 0$ and various values of the number density N .

4.1.2 Effect of Control Field Strength and Spontaneous Emission

We investigate the influence of the amplitude of the control Rabi frequency on the transparency window of the imaginary part of the susceptibility. The behavior of the imaginary part of susceptibility in terms of the probe laser detuning for $\Omega_{py} = 0.1\text{MHz}$, $\gamma_0 = \gamma_1 = 3.03\text{MHz}$, $\Delta_c = 0$, $N = 10^{24}m^{-3}$ is sketched in Fig. 4.8 for different values of Ω_{cy} . From Fig. 4.8, one can see that the EIT transparency window is wider when Ω_{cy} increases.

Figure 4.9 shows the behavior of the imaginary part of the susceptibility versus the probe laser detuning for various spontaneous decay rates $\gamma_0 = \gamma_1 = \gamma$. As one can see from Fig. 4.9, the EIT transparency window is slightly narrowed as the spontaneous decay

rate γ increases. Our findings are in agreement with the observation made in [29], where an increase in the number density directly correlates with an elevation in spontaneous emission.

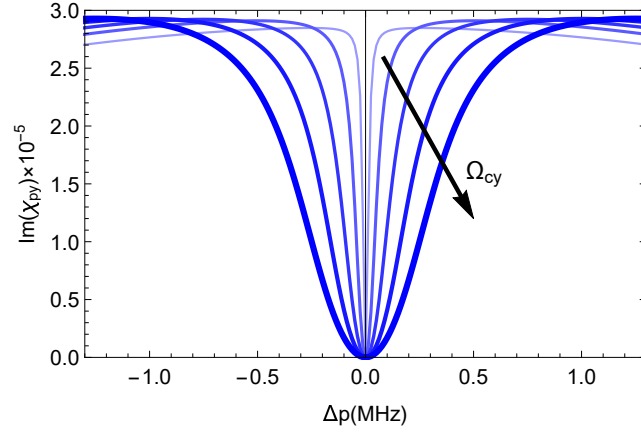


FIGURE 4.8: The imaginary parts of the susceptibility as a function of probe laser detuning for $\Omega_{py} = 0.1\text{MHz}$, $\gamma_0 = \gamma_1 = 3.03\text{MHz}$, $\Delta_c = 0$, $N = 10^{24}m^{-3}$ and various values of the control field Rabi frequency Ω_{cy} . The curves from top to down correspond to $\Omega_{cy} = 0.5, 1, 1.5, 2$ and 2.5 MHz. This strength is well below the limit when the approximations become invalid.

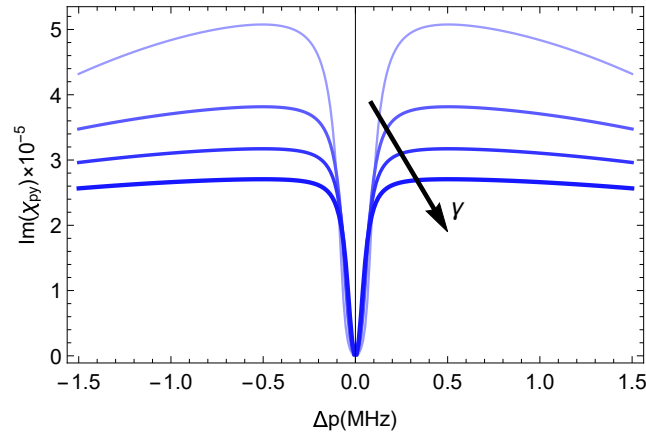


FIGURE 4.9: The imaginary parts of the susceptibility as a function of probe laser detuning for $\Omega_{py} = 0.1\text{MHz}$, $\Omega_{cy} = 1\text{MHz}$, $\Delta_c = 0$, $N = 10^{24}$ and various values of the spontaneous emission $\gamma_0 = \gamma_1 = \gamma$. The curves from top to down correspond to $\gamma = 0.5, 1.5, 2.5$ and 3.5 MHz.

4.2 Modelling EIT in an Atomic Ensemble with a Pulsed Probe

Up to now, we have considered an ensemble of three-level Λ atomic systems coupled by two monochromatic incident laser beams, where the interatomic interactions are taken into account in the decoherence terms. Now, we study the propagation of a Gaussian probe pulse through an atomic medium inspired by the treatment in Ref. [47]. In this work, they considered an ensemble of non-interacting three levels atoms in the ladder configuration. Because the excited state has only one direction, they assumed that the electric field is polarized in only one direction.

In my work, I make calculations for the ensemble of 3LAS with a multi-directional excited state where it's assumed that the scattering from the neighboring atoms is influencing. When the probe pulse enters the atomic medium, its propagation is governed by Maxwell's equations in the presence of the macroscopic polarization current. In the following, we find the Maxwell electric field equation in the so-called Slowly Varying Approximation [48].

By taking curl from

$$\vec{\nabla} \times \vec{E}(\vec{r}, t) = -\mu_0 \dot{\vec{H}}(\vec{r}, t), \quad (4.6)$$

and using

$$\vec{\nabla} \times \vec{H}(\vec{r}, t) = \epsilon_0 \dot{\vec{E}}(\vec{r}, t) + \vec{J}(\vec{r}, t), \quad (4.7)$$

as well as the Gauss equation $\vec{\nabla} \cdot \vec{E}(\vec{r}, t) = 0$, one can obtain

$$\frac{1}{c^2} \frac{\partial^2}{\partial t^2} \vec{E}(\vec{r}, t) - \vec{\nabla}^2 \vec{E}(\vec{r}, t) = -\frac{1}{c^2 \epsilon_0} \frac{\partial}{\partial t} \vec{J}(\vec{r}, t), \quad (4.8)$$

where the relation $c = 1/\sqrt{\mu\epsilon}$ has been used. In the literature, $\mu = \mu_0$ and ϵ has taken to be ϵ_0 . Due to the fact that the current density is expressed in terms of the macroscopic polarization of a medium,

$$\vec{J}(\vec{r}, t) = \frac{\partial}{\partial t} \vec{P}(\vec{r}, t), \quad (4.9)$$

we have

$$\frac{1}{c^2} \frac{\partial^2}{\partial t^2} \vec{E}(\vec{r}, t) - \vec{\nabla}^2 \vec{E}(\vec{r}, t) = -\frac{1}{c^2 \epsilon_0} \frac{\partial^2}{\partial t^2} \vec{P}(\vec{r}, t). \quad (4.10)$$

In our model, the electric field is polarized along the y -axis and is propagating in the z direction. Therefore,

$$\begin{aligned} E(t, z) &= E_0(t, z) \cos(\omega t - kz) \\ &= E_0(t, z)/2 \left(e^{-i\omega t + ikz} + e^{i\omega t - ikz} \right), \end{aligned} \quad (4.11)$$

with the wave vector $k = \omega/c$ and an amplitude $E_0(t, z)$ which depends on time as well as space z . By substituting the above electric field into the left-hand side of Eq. (4.10), we arrive at the expression

$$\begin{aligned} \frac{1}{c^2} \frac{\partial^2}{\partial t^2} E_0(t, z) \cos(\omega t - kz) - \frac{\partial^2}{\partial z^2} E_0(t, z) \cos(\omega t - kz) - \frac{2\omega}{c^2} \frac{\partial}{\partial t} E_0(t, z) \sin(\omega t - kz) \\ - 2k \frac{\partial}{\partial z} E_0(t, z) \sin(\omega t - kz) = -\frac{1}{c^2 \epsilon_0} \frac{\partial^2}{\partial t^2} P(t, z). \end{aligned} \quad (4.12)$$

Then, by applying the slowly-varying approximation:

$$\partial^2 / \partial t^2 E_0(t, z) \ll 2\omega \partial / \partial t E_0(t, z), \quad \partial^2 / \partial z^2 E_0(t, z) \ll 2k \partial / \partial z E_0(t, z),$$

the equation (4.12) becomes

$$\left(\frac{1}{c} \frac{\partial}{\partial t} E_0(t, z) + \frac{\partial}{\partial z} E_0(t, z) \right) \sin(\omega t - kz) = \frac{1}{2c\epsilon_0\omega} \frac{\partial^2}{\partial t^2} P(t, z). \quad (4.13)$$

For the probe electric field in the long-wavelength limit, this yields

$$\left(\frac{1}{c} \frac{\partial}{\partial t} E_{py}(t, z) + \frac{\partial}{\partial z} E_{py}(t, z) \right) \sin(\omega_p t) = \frac{1}{2c\epsilon_0\omega_p} \frac{\partial^2}{\partial t^2} P_y(t, z). \quad (4.14)$$

The component of macroscopic polarisation along the y -axis is obtained as the expectation value of an electric dipole moment operator

$$\begin{aligned} P_y &= N \text{Tr}(\rho \hat{\mu}_y), \\ &= N \mu_{02y} \frac{1}{2} e^{i\omega_p t} \rho_{02y} + N \mu_{02y} \frac{1}{2} e^{-i\omega_p t} \rho_{2y0}, \end{aligned} \quad (4.15)$$

where ρ_{02y} and ρ_{2y0} are the density matrix elements. By inserting this into the right-hand

side of Eq. (4.14), we obtain

$$\begin{aligned} & \left(\frac{1}{c} \frac{\partial}{\partial t} E_{py}(t, z) + \frac{\partial}{\partial z} E_{py}(t, z) \right) \sin(\omega_p t) = -\frac{N\mu_{02y}\omega_p}{4c\epsilon_0} (e^{i\omega_p t} \rho_{02y} + e^{-i\omega_p t} \rho_{2y0}) \\ & + \frac{iN\mu_{02y}}{2c\epsilon_0} \left(e^{i\omega_p t} \frac{\partial}{\partial t} \rho_{02y} - e^{-i\omega_p t} \frac{\partial}{\partial t} \rho_{2y0} \right) + \frac{N\mu_{02y}}{4c\epsilon_0\omega_p} (e^{i\omega_p t} \frac{\partial^2}{\partial t^2} \rho_{02y} + e^{-i\omega_p t} \frac{\partial^2}{\partial t^2} \rho_{2y0}). \end{aligned} \quad (4.16)$$

When the density matrix reaches steady state, this equation reduces to

$$\left(\frac{1}{c} \frac{\partial}{\partial t} E_{py}(t, z) + \frac{\partial}{\partial z} E_{py}(t, z) \right) \sin(\omega_p t) = -\frac{N\mu_{02y}\omega_p}{4c\epsilon_0} (e^{i\omega_p t} \rho_{02y} + e^{-i\omega_p t} \rho_{2y0}). \quad (4.17)$$

By matching the coefficient of $\sin(\omega_p t)$ on both sides, we find

$$\left(\frac{1}{c} \frac{\partial}{\partial t} E_{py}(t, z) + \frac{\partial}{\partial z} E_{py}(t, z) \right) = \frac{N\mu_{02y}\omega_p}{2c\epsilon_0} \text{Im}(\rho_{02y}), \quad (4.18)$$

or equivalently

$$\left(\frac{1}{c} \frac{\partial}{\partial t} \Omega_{py}(t, z) + \frac{\partial}{\partial z} \Omega_{py}(t, z) \right) = \frac{N\mu_{02y}^2\omega_p}{2c\epsilon_0\hbar} \text{Im}(\rho_{02y}), \quad (4.19)$$

where the Rabi frequency, $\Omega_{py} = E_{pi}\mu_{02y}/\hbar$. Numerical solution of the above equation using these two variables (t and z) has been extensively studied in various research works, such as the Ref. [49].

In Ref. [47], the author solved these equations by making important simplifications. They changed the coordinates as [47]

$$\tau = t - z/c, \quad \xi = z, \quad (4.20)$$

which leads to change the derivatives as

$$\begin{aligned} \frac{\partial}{\partial t} &= \frac{\partial}{\partial \tau}, \\ \frac{\partial}{\partial z} &= -\frac{1}{c} \frac{\partial}{\partial \tau} + \frac{\partial}{\partial \xi}, \end{aligned} \quad (4.21)$$

one gets

$$\frac{\partial}{\partial \xi} \Omega_{py}(\tau, \xi) = \eta \text{Im}(\rho_{02y}), \quad (4.22)$$

where we have defined $\eta = N\mu_{02y}^2\omega_p/(2c\epsilon_0\hbar)$. In Ref. [47], they assumed that the pulse's polarization occurs in just one direction; therefore, the equation is one-dimensional. This approach allowed their calculations to remain unaffected by the length of the medium.

In this work, we move away from the approximation of Eq. (4.11) and assume that the electric field can be polarized in all three directions. Then, using the slowly varying approximation and the same change in coordinates as in Ref. [47], the set of equations that must be simultaneously solved is

$$\begin{aligned}\frac{\partial}{\partial\xi}\Omega_{py}(\tau, \xi) &= \eta\text{Im}(\rho_{02y}), \\ \frac{\partial}{\partial\xi}\Omega_{px}(\tau, \xi) &= \eta\text{Im}(\rho_{02x}), \\ \frac{\partial}{\partial\xi}\Omega_{pz}(\tau, \xi) &= \eta\text{Im}(\rho_{02z}),\end{aligned}\tag{4.23}$$

where $\mu_{02x} = \mu_{02y} = \mu_{02z}$ has been used for the dipole moment element. To explore the dynamics of the probe pulse in an atomic medium, we need to solve the above Maxwell's equations (4.23) coupled to the Liouville-von Neumann equations (3.41), which take the following forms in the new coordinates Eq. (4.20)

$$\frac{\partial}{\partial\tau}\rho(\tau, \xi) = -\frac{i}{\hbar}[H_{ens}, \rho(\tau, \xi)] - L(\rho(\tau, \xi)),\tag{4.24}$$

with the Lindblad superoperator $L(\rho(\tau, \xi))$ given by

$$L(\rho(\tau, \xi)) = \sum_{i=2x,2y,2z} \sum_{j=0,1} \frac{\gamma_{ij}}{2} \left(\sigma_{ij}^\dagger \sigma_{ij} \rho + \rho \sigma_{ij}^\dagger \sigma_{ij} - 2\sigma_{ij} \rho \sigma_{ij}^\dagger \right).\tag{4.25}$$

Note that a multi-directional basis is used here which is different from Ref. [47] that considers non-interacting atoms in the ensemble. We consider the initial condition for the Liouville-von Neumann in the form

$$\rho_{00}(\tau \rightarrow -\infty, \xi) = 1, \quad \rho_{11}(\tau \rightarrow -\infty, \xi) = 0,$$

$$\rho_{2x2x}(\tau \rightarrow -\infty, \xi) = 0, \quad \rho_{2y2y}(\tau \rightarrow -\infty, \xi) = 0, \quad \rho_{2z2z}(\tau \rightarrow -\infty, \xi) = 0.\tag{4.26}$$

For the incident probe, we assume a Gaussian pulse shape with a maximum amplitude Ω_{py0}

$$\Omega_{py}(\tau, \xi = 0) = \Omega_{py0} e^{-t^2/(2\Delta\tau^2)}, \quad (4.27)$$

where $\Delta\tau$ is the pulse duration. For each number density N , the pulse duration $\Delta\tau$ is calculated from the FWHM values plotted in Fig. 4.5 using

$$\Delta\tau = 2\sqrt{2 \ln 2}/\text{FWHM}. \quad (4.28)$$

The results of calculations for the propagation of probe pulse for the ensemble model under various conditions are represented in Figs. (4.10) and (4.11) where I choose a length of the medium of $L = 500$ and $58.5nm$ which extends from $\xi = 0$ to $\xi = L$. In Fig. (4.10), I consider an initial incident pulse with a maximum amplitude of $\Omega_{py0} = 0.1\text{MHz}$ and a width of $\Delta\tau = 14.52\mu s$, while other parameters are fixed to $\Omega_{cy} = 1\text{MHz}$, $\gamma_0 = \gamma_1 = 3.03\text{MHz}$, $N = 10^{16}m^{-3}$, $\Delta_p = 0$, $\Delta_c = 0$ and $L = 500nm$. In this case, we can obviously see that the output pulse shape is identical to the shape of the initial pulse in all directions.

When the number density of atoms increases to $N = 10^{20}m^{-3}$ for the length of the medium $L = 58.5nm$ in Fig. (4.11), the output pulse is reduced in amplitude, where the input pulse duration remains almost constant. In addition, the maximum of the output pulse is shifted compared to the input one. While it is $1/e$ of the maximum value in the initial incident pulse. Also, one can see that the output probe laser pulse is severely distorted.

To further clarify the distortion of the output probe pulse within the medium, I investigate the length scale over which the maximum of the output pulse becomes $1/e$ of the maximum of the input pulse,

$$\text{Max}[\Omega(\tau, \xi = L_\alpha)] = \Omega_{py0}/e, \quad (4.29)$$

where I call L_α an absorption length. To do so, in Fig. (4.12), I show the behavior of the absorption length L_α as a function of the number density N . Here, the values of the parameters are $\Omega_{py0} = 0.1\text{MHz}$, $\Omega_{cy} = 1\text{MHz}$, $\gamma_0 = \gamma_1 = 3.03\text{MHz}$, $\Delta_p = 0$, $\Delta_c = 0$. As can be seen from Fig. (4.12), the absorption length decreases linearly in logarithmic scale

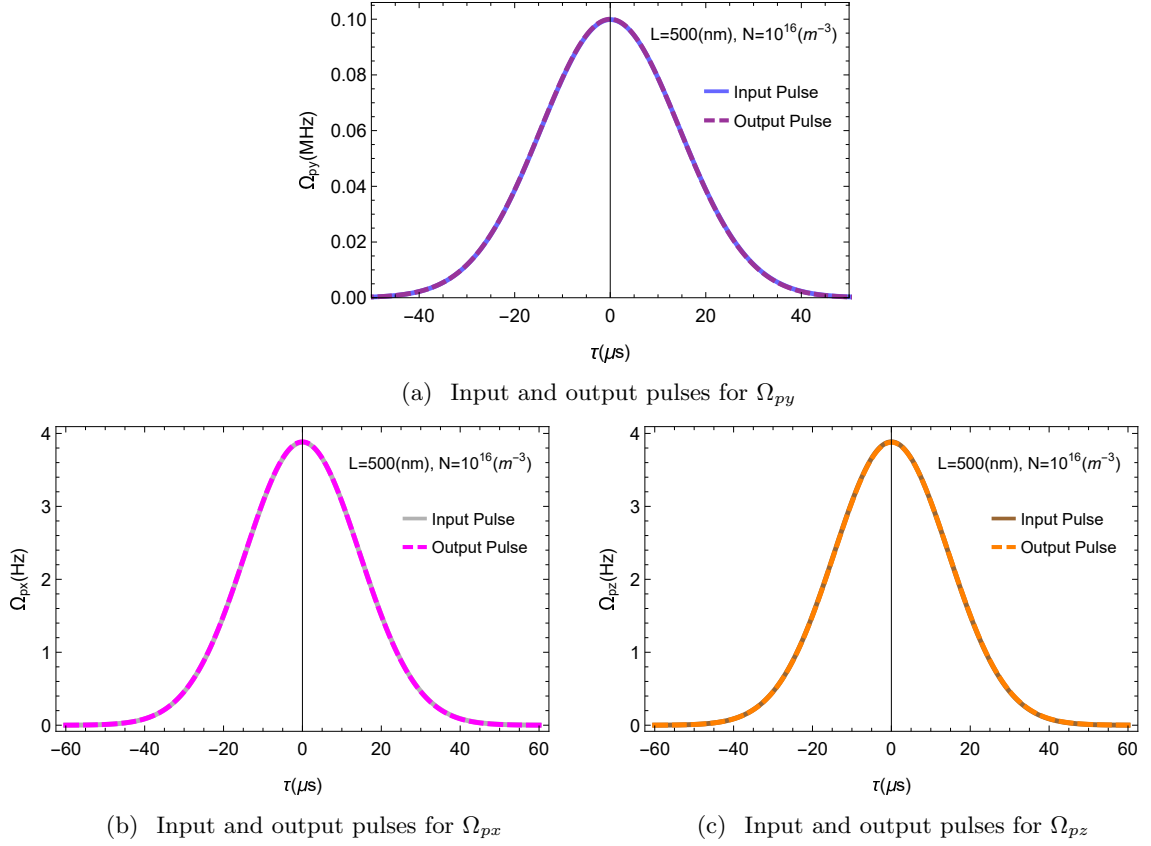


FIGURE 4.10: The probe laser field for the input and output pulses in all directions. The parameters used are $\Omega_{py0} = 0.1\text{MHz}$, $\Omega_{cy} = 1\text{MHz}$, $\gamma_0 = \gamma_1 = 3.03\text{MHz}$, $N = 10^{16}m^{-3}$, $\Delta_p = 0$, $\Delta_c = 0$, $\Delta\tau = 14.52\mu s$ and $L = 500nm$. The input and output pulses match with each other. Note that the scale of the y -axis in figures (b) and (c) is Hz. The scattering in the x and z directions is very small.

with number density from 10^{13} to $10^{22} m^{-3}$. Compared to the FWHM graph 4.5, where we observed a linear decrease at larger N values, in this case, the decrease is exponential. This means that as N increases, the EIT conditions are sustained for much larger N values. Nevertheless, for these increased N values, the length over which the pulse propagates experiences a significant reduction.

Summary

In this chapter, I present two models. The first model is a single-particle model, which indicates that the expected EIT (Electromagnetically Induced Transparency) behavior persists up to a considerable $N = 10^{23}m^{-3}$. In contrast, the second model, referred to as the pulse model, reveals that EIT behavior is observed at significantly lower number densities.

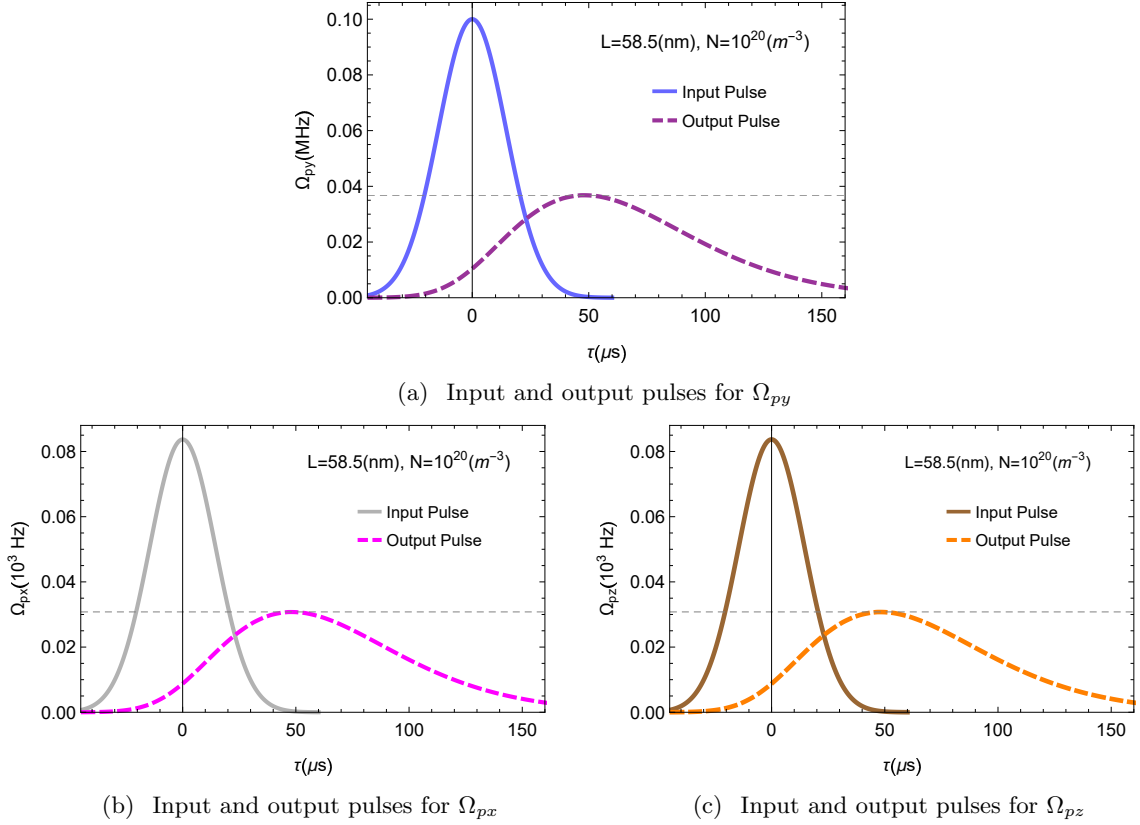


FIGURE 4.11: The probe laser field for the input and output pulses in all directions. The parameters used are $\Omega_{py0} = 0.1\text{MHz}$, $\Omega_{cy} = 1\text{MHz}$, $\gamma_0 = \gamma_1 = 3.03\text{MHz}$, $N = 10^{20}\text{m}^{-3}$, $\Delta_p = 0$, $\Delta_c = 0$, $\Delta\tau = 14.53\mu\text{s}$ and $L = 58.5\text{nm}$. The horizontal thin gray dashed line denotes $1/e$ of a maximum of the initial input pulse.

This distinction arises due to inter-particle scattering effects. In summary, the first model exhibits an EIT window at a number density of $N = 10^{23}\text{m}^{-3}$, while the second model shows that meaningful absorption can only be achieved at much lower densities. Consequently, despite the favorable transparency window obtained by increasing the number density in the first model, the pulse does not manifest any significant effect; rather, it continues to be absorbed by the system in this particular scenario.

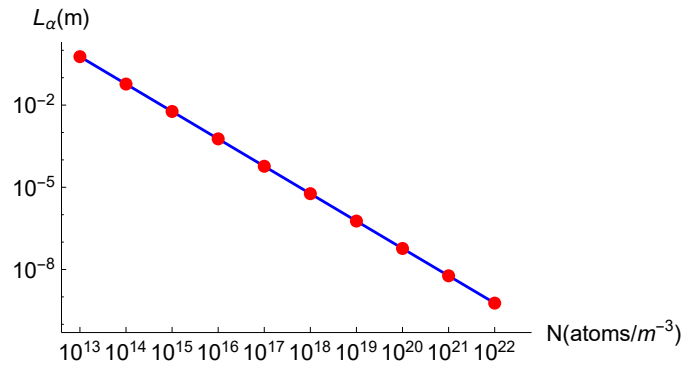


FIGURE 4.12: The behaviors of absorption length L_α versus number density N . The parameters used are $\Omega_{py0} = 0.1\text{MHz}$, $\Omega_{cy} = 1\text{MHz}$, $\gamma_0 = \gamma_1 = 3.03\text{MHz}$, $\Delta_p = 0$, $\Delta_c = 0$. We use the logarithmic scale for the vertical axis.

Chapter 5

Conclusion

Throughout this thesis, my primary focus was on exploring the phenomena of Electromagnetically Induced Transparency (EIT) in an ensemble of three-level Λ systems (3LAS) with a multi-directional excited state. The model I developed is based on the nearest neighbour interatomic interaction of three-level Λ atoms within the ensemble. Notably, each member of the ensemble behaves as an individual quantum emitter capable of spontaneous radiation in all directions, even perpendicular to the incident beam. This aspect becomes significant as radiation fields in all directions can excite atoms with different orientations of the dipole moment, a crucial factor that has not been thoroughly studied in previous works.

The central goal of my research was to study the influence of these effects on the EIT behavior in atomic ensembles, a topic largely unexplored in the existing literature. To achieve this, I conducted a detailed analysis of the optical properties of the ensemble and compared them to those of a single atom. This comparative approach provided valuable insights into how the collective behavior of the ensemble affects the EIT phenomenon. Additionally, the study investigated a Gaussian probe pulse propagating in a three-level Λ medium with a multi-directional excited state, coupled to a monochromatic control field, exploring its potential applications in improving optical quantum memory.

I began by providing a review of the EIT phenomenon within a single three-level Λ system. By calculating the electric susceptibility of the probe field through the density matrix, I determined the transparency window and refractive index. Furthermore, I explored the

group velocity of the probe field within the medium. Next, I presented a methodology to model an ensemble of atomic systems using an effective single-particle model, considering decoherence terms such as effective spontaneous decay and dephasing rates. This laid the groundwork for investigating the EIT effect in the subsequent step. Finally, the modeling methodology was extended to the ensemble of 3LAS, leading to the presentation of two distinct models. The first model involved representing the ensemble as a single-particle density matrix with specific decoherence terms. This model enabled predictions of the transparency window and group velocity of a probe field, demonstrating the dependence on the ensemble's number density. Additionally, a model was extended for a probe field propagating through the ensemble in a slowly varying (field) approximation, yielding intriguing results concerning density dependence. The first model, a single-particle model, suggests that EIT behavior is expected to persist for a considerable number density of $N = 10^{23}m^{-3}$. In contrast, the second model, referred to as the pulse model, indicates that EIT behavior is observable and useful only at significantly lower number densities.

In conclusion, our analysis demonstrates that in an ensemble of three-level Λ systems (3LAS) with a multi-directional excited state and driven by two monochromatic fields, an EIT window is observed at a number density of $N = 10^{23}m^{-3}$. However, when a pulse is introduced in an ensemble of three-level Λ systems (3LAS) with a multi-directional excited state, meaningful absorption is achievable only at much lower number densities. Despite achieving a favorable transparency window by increasing the number density in the first model, the second model shows that EIT is not observed at high densities. These findings underscore the crucial role of density in shaping the EIT behavior and absorption characteristics of the system, providing valuable insights into the intricate dynamics of EIT phenomena in dense atomic ensembles.

5.1 Future Directions

In the pursuit of future directions, several key avenues can be explored to enhance our understanding of the Electromagnetically Induced Transparency (EIT) phenomena in the atomic ensemble with a multi-directional excited state. Firstly, utilizing the density matrix derived from the single particle model as a source offers a promising approach to investigate

its implications on the electric field at long distances.

Secondly, numerically solving the Maxwell-Lindblad equations for the entire atomic ensemble presents another fruitful direction. This computational approach will provide a deeper understanding of the dynamic interactions between the atoms and their surrounding environment, enabling a comprehensive exploration of the ensemble's behavior under diverse conditions. Additionally, conducting a comparative analysis between the numerical results obtained from the Maxwell-Lindblad equations for the ensemble and those obtained from the single particle model will be essential to validate the ensemble model's accuracy and efficacy. This comparative study will help discern any collective effects and deviations arising due to inter-particle interactions.

5.2 Limitations

This work has certain limitations that should be considered. The atomic ensemble model explored here may not be suitable for solids for two reasons. Firstly, the density of typical solids is high, at which the EIT behavior breaks down. Secondly, we have ignored the interatomic interactions present in solids. Note that experiments claiming to have observed EIT in solids [25] are typically conducted in solids doped with color centers. As a result, the number density of the color centers is significantly lower than that of the solid itself. However, these experiments may offer a means of testing my hypothesis that the number density of the color centers can be altered by adjusting the doping concentration.

Another limitation lies in the assumption of a constant control field, typically represented as a pulse. In reality, control fields can vary over time; however, the difference in numerical predictions is not significant.

Lastly, the assumption of a perfect initial population distribution ($\rho_{00} = 1$) is not accurate due to the presence of two ground states with frequencies very close to each other (approximately 6000 MHz). This discrepancy could potentially impact the model's accuracy. To enhance the model's reliability, one can begin by considering varying initial state populations.

Using my methods, we can significantly advance our comprehension of EIT phenomena

and collective behaviors in quantum systems, opening up exciting possibilities for practical applications in diverse fields, including optical quantum memory.

Appendix A

The Interaction Picture with the Rotating Wave Approximation (RWA)

Quantum systems' dynamics are defined by their time-dependent density matrix when an external field is present. These dynamics are predominantly dictated by oscillations correlated with incident fields' frequency. To analyze slow dynamics, such as quantum interference or Rabi oscillations, it is necessary to examine the systems from a rotating perspective that is parallel to the incident field's frequency. When applying this approach within the context of N -level quantum system, it is ideal to ascertain an $N \times N$ rotation matrix that is unitary (U) as this approach can rotate the system effectively so as to achieve the necessary frame [41]. Then, executing the transformation of the unitary can determine the interaction Hamiltonian

$$H_I = U H U^\dagger - i\hbar U \dot{U}^\dagger. \quad (\text{A.1})$$

When identifying systems' ideal equations, the primary issue is securing an accurate determination of the U matrix. The U choice is clearly established and recognized for atoms that have two or three levels [50]; however, multi-level systems with energy levels that are non-degenerate are far more difficult to ascertain. In three-level systems and three-level systems with a multi-directional excited state, the transformation matrix we employ

comprises two terms: $\exp(-i\omega_j t)$ and $\exp(-i\omega_{i,j} t)$, where the rapid rotation caused by the transition frequency $\omega_{i,j}$.

The Rotating Wave Approximation (RWA) utilizes to reduce oscillation frequencies in the system through dividing terms into high and low-frequency. In this approximation the counter rotating terms are ignored.

A.1 Three-level Λ Systems

In the case of a three-level Λ atomic system interacting with two deriving fields, the total Hamiltonian is

$$H = - \begin{pmatrix} -\hbar\omega_0 & 0 & \mu_{02}E_p(e^{-i\omega_p t} + e^{i\omega_p t})/2 \\ 0 & -\hbar\omega_1 & \mu_{12}E_c(e^{-i\omega_c t} + e^{i\omega_c t})/2 \\ \mu_{02}E_p(e^{-i\omega_p t} + e^{i\omega_p t})/2 & \mu_{12}E_c(e^{-i\omega_c t} + e^{i\omega_c t})/2 & -\hbar\omega_2 \end{pmatrix}. \quad (\text{A.2})$$

Using excited state as a reference level, the unitary transformation matrix is given by

$$U = \begin{pmatrix} e^{-i(\omega_p + \omega_2)t} & 0 & 0 \\ 0 & e^{-i(\omega_c + \omega_2)t} & 0 \\ 0 & 0 & e^{-i\omega_2 t} \end{pmatrix}, \quad (\text{A.3})$$

After neglecting of all high-frequency terms, we find the Hamiltonian in the interaction picture after RWA

$$H_{RWA} = -\frac{\hbar}{2} \begin{pmatrix} -2\Delta_p & 0 & \Omega_p \\ 0 & -2\Delta_c & \Omega_c \\ \Omega_p & \Omega_c & 0 \end{pmatrix}, \quad (\text{A.4})$$

Where $\Delta_p = \omega_p - \omega_2 + \omega_0$ and $\Delta_c = \omega_c - \omega_2 + \omega_1$ are the laser detunings. Note that the prime is dropped for convenience.

A.2 Three-level Λ Systems with a Multi-directional excited state

The Hamiltonian of a three-level system with a multi-directional excited state, including three degenerate excited states, two ground states that are close in energy, is

$$H = -\hbar \begin{pmatrix} -\omega_0 & 0 & \Omega_{px} \cos(\omega_p t) & \Omega_{py} \cos(\omega_p t) & \Omega_{pz} \cos(\omega_p t) \\ 0 & \omega_1 & -\Omega_{cx} \cos(\omega_c t) & \Omega_{cy} \cos(\omega_c t) & \Omega_{cz} \cos(\omega_c t) \\ \Omega_{px} \cos(\omega_p t) & \Omega_{cx} \cos(\omega_c t) & -\omega_2 & 0 & 0 \\ \Omega_{py} \cos(\omega_p t) & \Omega_{cy} \cos(\omega_c t) & 0 & -\omega_2 & 0 \\ \Omega_{pz} \cos(\omega_p t) & \Omega_{cz} \cos(\omega_c t) & 0 & 0 & -\omega_2 \end{pmatrix}. \quad (\text{A.5})$$

In this case, the unitary transformation matrix is taken

$$U = \begin{pmatrix} e^{-i(\omega_p+\omega_2)t} & 0 & 0 & 0 & 0 \\ 0 & e^{-i(\omega_c+\omega_2)t} & 0 & 0 & 0 \\ 0 & 0 & e^{-i\omega_2 t} & 0 & 0 \\ 0 & 0 & 0 & e^{-i\omega_2 t} & 0 \\ 0 & 0 & 0 & 0 & e^{-i\omega_2 t} \end{pmatrix}, \quad (\text{A.6})$$

By adopting the rotating wave approximation, we have the Hamiltonian in the rotating frame as

$$H_{RWA} = -\frac{\hbar}{2} \begin{pmatrix} -2\Delta_p & 0 & \Omega_{px} & \Omega_{py} & \Omega_{pz} \\ 0 & -2\Delta_c & \Omega_{cx} & \Omega_{cy} & \Omega_{cz} \\ \Omega_{px} & \Omega_{cx} & 0 & 0 & 0 \\ \Omega_{py} & \Omega_{cy} & 0 & 0 & 0 \\ \Omega_{pz} & \Omega_{cz} & 0 & 0 & 0 \end{pmatrix}, \quad (\text{A.7})$$

where $\Delta_p = \omega_p - \omega_2 + \omega_0$ and $\Delta_c = \omega_c - \omega_2 + \omega_1$ are the detunings of the control and probe field frequencies from atomic resonance frequencies.

Appendix B

Lindblad-von Neumann Equation

The density matrix $\hat{\rho}$ can be expressed as the outer product of the wave function with its complex conjugate

$$\hat{\rho} = |\psi\rangle\langle\psi|. \quad (\text{B.1})$$

By applying a unitary transformation U , the transformed wave function is given as follows

$$|\psi'\rangle = U|\psi\rangle, \quad (\text{B.2})$$

where the prime indicates the transformed frame. The relation between the transformed density matrix and the original density matrix is determined by

$$\rho = U^\dagger \rho' U. \quad (\text{B.3})$$

The Lindblad-von Neumann equation is

$$\dot{\rho} = -\frac{i}{\hbar}[H, \rho] - L(\rho) \quad (\text{B.4})$$

in which the superoperator representing decoherence processes

$$L(\rho) = \sum_d \frac{\gamma_d}{2} \left(\sigma_d^\dagger \sigma_d \rho + \rho \sigma_d^\dagger \sigma_d - 2\sigma_d \rho \sigma_d^\dagger \right). \quad (\text{B.5})$$

Now, by substituting the density matrix (B.3) into the above Lindblad-von Neumann equa-

tion, we get

$$\frac{\partial}{\partial t} (U^\dagger \rho' U) = -\frac{i}{\hbar} [H, U^\dagger \rho' U] - L(U^\dagger \rho' U). \quad (\text{B.6})$$

The left side of the above equation becomes

$$\frac{\partial}{\partial t} (U^\dagger \rho' U) = U^\dagger \dot{\rho}' U + \dot{U}^\dagger \rho' U + U^\dagger \rho' \dot{U}. \quad (\text{B.7})$$

For the right side of the equation (B.6), we have

$$[H, U^\dagger \rho' U] = H U^\dagger \rho' U - U^\dagger \rho' U H = U^\dagger U H U^\dagger \rho' U - U^\dagger \rho' U H U^\dagger U. \quad (\text{B.8})$$

After doing some calculations, we arrive at

$$U^\dagger \dot{\rho}' U = -\frac{i}{\hbar} U^\dagger [U H U^\dagger - i \hbar U \dot{U}^\dagger, \rho'] U - L(U^\dagger \rho' U). \quad (\text{B.9})$$

By the definition

$$H_T = U H U^\dagger - i \hbar U \dot{U}^\dagger, \quad (\text{B.10})$$

the above equation is written as follows

$$U^\dagger \dot{\rho}' U = -\frac{i}{\hbar} U^\dagger [H_T, \rho'] U - L(U^\dagger \rho' U). \quad (\text{B.11})$$

Then, we multiply by U from the left side and U^\dagger from the right side,

$$\dot{\rho}' = -\frac{i}{\hbar} [H_T, \rho'] - U L(U^\dagger \rho' U) U^\dagger. \quad (\text{B.12})$$

In the transformed frame, the Lindblad operators take the form

$$\sigma'_d = U \sigma_d U^\dagger. \quad (\text{B.13})$$

Thus, the equation (B.12) yields

$$\dot{\rho}' = -\frac{i}{\hbar} [H_T, \rho'] - L(\rho'), \quad (\text{B.14})$$

with

$$L(\rho') = \sum_d \frac{\gamma_d}{2} \left(\sigma_d'^{\dagger} \sigma_d' \rho' + \rho' \sigma_d'^{\dagger} \sigma_d' - 2 \sigma_d' \rho' \sigma_d'^{\dagger} \right). \quad (\text{B.15})$$

Appendix C

Scaling Parameters

In quantum systems employing the RWA approximation, we can leverage the scaling evolution of the systems to reduce the number of free parameters. With this scaling approach, the Lindblad-Von Neumann master equation,

$$\dot{\rho} = -\frac{i}{\hbar} [H_{RWA}, \rho] - L(\rho), \quad (\text{C.1})$$

is then transformed

$$\dot{\rho}/S = -\frac{i}{\hbar} [H_{RWA}/S, \rho] - L(\rho)/S, \quad (\text{C.2})$$

$$\dot{\rho}' = -\frac{i}{\hbar} [H'_{RWA}, \rho] - L'(\rho). \quad (\text{C.3})$$

By using the chosen $S = 1\text{MHz}$ as a unit, we can define other system parameters in a consistent manner

$$\begin{aligned} \gamma &= \gamma' S, \\ \Delta &= \Delta' S, \\ \Omega_i &= \Omega'_i S, \\ t &= t' \frac{1}{S}, \\ \omega_i &= \omega'_i S. \end{aligned} \quad (\text{C.4})$$

Rates given in Chapters 2 and 4 are all scaled using this approach.

Bibliography

- [1] Michael Fleischhauer, Atac Imamoglu, and Jonathan P Marangos. Electromagnetically induced transparency: Optics in coherent media. *Reviews of Modern Physics*, 77(2):633, 2005.
- [2] OA Kocharovskaya and Ya I Khanin. Coherent amplification of an ultrashort pulse in a three-level medium without a population inversion. *Soviet Journal of Experimental and Theoretical Physics Letters*, 48:630, 1988.
- [3] Stephen E Harris. Lasers without inversion: Interference of lifetime-broadened resonances. *Physical Review Letters*, 62(9):1033, 1989.
- [4] K-J Boller, A Imamoglu, and Stephen E Harris. Observation of electromagnetically induced transparency. *Physical Review Letters*, 66(20):2593, 1991.
- [5] Julio Gea-Banacloche, Yong-qing Li, Shao-zheng Jin, and Min Xiao. Electromagnetically induced transparency in ladder-type inhomogeneously broadened media: Theory and experiment. *Physical Review A*, 51(1):576, 1995.
- [6] Ray-Yuan Chang, Wei-Chia Fang, Zong-Syun He, Bai-Cian Ke, Pei-Ning Chen, and Chin-Chun Tsai. Doubly dressed states in a ladder-type system with electromagnetically induced transparency. *Physical Review A*, 76(5):053420, 2007.
- [7] George R Welch, GG Padmabandu, Edward S Fry, Mikhail D Lukin, Dmitri E Nikonov, Frank Sander, Marlan O Scully, Antoin Weis, and Frank K Tittel. Observation of v -type electromagnetically induced transparency in a sodium atomic beam. *Foundations of Physics*, 28(4):621–638, 1998.

-
- [8] Ying Wu and Xiaoxue Yang. Electromagnetically induced transparency in v -, λ -, and cascade-type schemes beyond steady-state analysis. *Physical Review A*, 71(5):053806, 2005.
- [9] F Ghafoor and RG Nazmitdinov. Triplet absorption spectroscopy and electromagnetically induced transparency. *Journal of Physics B: Atomic, Molecular and Optical Physics*, 49(17):175502, 2016.
- [10] AS Zibrov, CY Ye, YV Rostovtsev, AB Matsko, and MO Scully. Observation of a three-photon electromagnetically induced transparency in hot atomic vapor. *Physical Review A*, 65(4):043817, 2002.
- [11] Khairul Islam, Dipankar Bhattacharyya, Arindam Ghosh, Debasish Biswas, and Amitava Bandyopadhyay. Study on probe field propagation in the presence of control and coupling fields through a four-level n -type atomic system. *Journal of Physics B: Atomic, Molecular and Optical Physics*, 50(21):215401, 2017.
- [12] GS Agarwal and W Harshawardhan. Inhibition and enhancement of two photon absorption. *Physical Review Letters*, 77(6):1039, 1996.
- [13] Laleh Safari, Denys Iablonskyi, and Filippo Fratini. Double-electromagnetically induced transparency in a y -type atomic system. *The European Physical Journal D*, 68(2):1–8, 2014.
- [14] BP Hou, SJ Wang, WL Yu, and WL Sun. Double electromagnetically induced two-photon transparency in a five-level atomic system. *Physics Letters A*, 352(4-5):462–466, 2006.
- [15] HR Askari and M Moezzi. The generation of the double windows of eit in w -type 4-level cylindrical quantum dot. *Optik*, 126(23):4612–4620, 2015.
- [16] Arindam Ghosh, Khairul Islam, Dipankar Bhattacharyya, and Amitava Bandyopadhyay. Revisiting the four-level inverted- y system under both doppler-free and doppler-broadened conditions: an analytical approach. *Journal of Physics B: Atomic, Molecular and Optical Physics*, 49(19):195401, 2016.
- [17] Arindam Ghosh, Khairul Islam, Suman Mondal, Dipankar Bhattacharyya, Nikhil Pal, and Amitava Bandyopadhyay. A study on electromagnetically induced transparency

- and velocity selective optically pumped absorption in an eight-level inverted y-type atomic system. *Journal of Physics B: Atomic, Molecular and Optical Physics*, 51(14):145501, 2018.
- [18] MM Hossain, S Mitra, B Ray, and PN Ghosh. High contrast electromagnetically induced transparency in a nitrogen filled rb vapour cell. *Laser Physics*, 19(10):2008–2013, 2009.
- [19] Verònica Ahufinger, R Corbalán, F Cataliotti, Sven Burger, F Minardi, and C Fort. Electromagnetically induced transparency in a Bose–Einstein condensate. *Optics Communications*, 211(1-6):159–165, 2002.
- [20] Irina Novikova, Ronald L Walsworth, and Yanhong Xiao. Electromagnetically induced transparency-based slow and stored light in warm atoms. *Laser & Photonics Reviews*, 6(3):333–353, 2012.
- [21] Andrey B Matsko, Olga Kocharovskaya, Yuri Rostovtsev, George R Welch, Alexander S Zibrov, and Marlan O Scully. Slow, ultraslow, stored, and frozen light. *Advances in Atomic Molecular and Optical Physics*, 46:191–242, 2001.
- [22] Michael Fleischhauer and Mikhail D Lukin. Dark-state polaritons in electromagnetically induced transparency. *Physical Review Letters*, 84(22):5094, 2000.
- [23] MD Lukin and Ataç Imamoğlu. Controlling photons using electromagnetically induced transparency. *Nature*, 413(6853):273–276, 2001.
- [24] Lijun Ma, Oliver Slattery, and Xiao Tang. Optical quantum memory based on electromagnetically induced transparency. *Journal of Optics*, 19(4):043001, 2017.
- [25] Mark C Phillips and Hailin Wang. Exciton spin coherence and electromagnetically induced transparency in the transient optical response of GaAs quantum wells. *Physical Review B*, 69(11):115337, 2004.
- [26] S Marcinkevičius, A Gushterov, and JP Reithmaier. Transient electromagnetically induced transparency in self-assembled quantum dots. *Applied Physics Letters*, 92(4), 2008.

- [27] Ofer Firstenberg, M Shuker, Nir Davidson, and A Ron. Elimination of the diffraction of arbitrary images imprinted on slow light. *Physical Review Letters*, 102(4):043601, 2009.
- [28] H Li, H Chen, MA Gubin, YV Rostovtsev, VA Sautenkov, and MO Scully. Observation of electromagnetically induced transparency in cesium molecules. *Laser Physics*, 20:1725–1728, 2010.
- [29] CS DiLoreto and C Rangan. Single-particle model of a strongly driven, dense, nanoscale quantum ensemble. *Physical Review A*, 97(1):013812, 2018.
- [30] Bihui Zhu, John Cooper, Jun Ye, and Ana Maria Rey. Light scattering from dense cold atomic media. *Physical Review A*, 94(2):023612, 2016.
- [31] AS Kuraptsev and IM Sokolov. Spontaneous decay of an atom excited in a dense and disordered atomic ensemble: Quantum microscopic approach. *Physical Review A*, 90(1):012511, 2014.
- [32] Maxim Sukharev and Abraham Nitzan. Numerical studies of the interaction of an atomic sample with the electromagnetic field in two dimensions. *Physical Review A*, 84(4):043802, 2011.
- [33] Heinz-Peter Breuer and Francesco Petruccione. *The Theory of Open Quantum Systems*. Oxford University Press, USA, 2002.
- [34] Peiru He, Phoebe M Tengdin, Dana Z Anderson, Ana Maria Rey, and Murray Holland. Sub-doppler laser cooling using electromagnetically induced transparency. *Physical Review A*, 95(5):053403, 2017.
- [35] Robert W Boyd and Daniel J Gauthier. “slow” and “fast” light. 2002.
- [36] Robert W Boyd. Slow and fast light: fundamentals and applications. *Journal of Modern Optics*, 56(18-19):1908–1915, 2009.
- [37] Robert W Boyd. Material slow light and structural slow light: similarities and differences for nonlinear optics. *JOSA B*, 28(12):A38–A44, 2011.
- [38] Lene Vestergaard Hau. Optical information processing in bose–einstein condensates. *Nature Photonics*, 2(8):451–453, 2008.

- [39] AV Turukhin, VS Sudarshanam, MS Shahriar, JA Musser, BS Ham, and PR Hemmer. Observation of ultraslow and stored light pulses in a solid. *Physical Review Letters*, 88(2):023602, 2001.
- [40] Chien Liu, Zachary Dutton, Cyrus H Behroozi, and Lene Vestergaard Hau. Observation of coherent optical information storage in an atomic medium using halted light pulses. *Nature*, 409(6819):490–493, 2001.
- [41] CS DiLoreto and C Rangan. Decoherent excitation of transverse free currents in dielectric liquids via inter-molecular interactions. *Frontiers in Physics*, page 389, 2021.
- [42] Allen Taflove, Susan C Hagness, and Melinda Picket-May. Computational electromagnetics: the finite-difference time-domain method. *The Electrical Engineering Handbook*, 3:629–670, 2005.
- [43] Qing H Liu. The pstd algorithm: A time-domain method requiring only two cells per wavelength. *Microwave and Optical Technology Letters*, 15(3):158–165, 1997.
- [44] Jean-Pierre Bérenger. Perfectly matched layer (pml) for computational electromagnetics. *Synthesis Lectures on Computational Electromagnetics*, 2(1):1–117, 2007.
- [45] A Fratalocchi, C Conti, and G Ruocco. Three-dimensional ab initio investigation of light-matter interaction in mie lasers. *Physical Review A*, 78(1):013806, 2008.
- [46] Lukas Novotny and Bert Hecht. *Principles of Nano-Optics*. Cambridge University Press, 2012.
- [47] Minh Dong Hoang, Ngoc Sau Vu, Xuan Khoa Dinh, Nguyen Huy Bang, et al. Propagation of a laser pulse in a three-level cascade atomic medium under conditions of electromagnetically induced transparency. *Photonics Letters of Poland*, 8(3):73–75, 2016.
- [48] Marlan O Scully and M Suhail Zubairy. *Quantum optics*, 1999.
- [49] Dong Sun, Zoe-Elizabeth Sariyanni, Sumanta Das, and Yuri V Rostovtsev. Propagation of 0π pulses in a gas of three-level atoms. *Physical Review A*, 83(6):063815, 2011.
- [50] David J Tannor. *Introduction to Quantum Mechanics: a Time-Dependent Perspective*. University Science Books, Sausalito, CA, United States, 2007.

Vita Auctoris

NAME: Sara Moezzi

PLACE OF BIRTH: Iran

YEAR OF BIRTH: 1988

EDUCATION: Islamic Azad University, B.Sc., Iran, 2011
Vali-e-Asr University of Rafsanjan, M.Sc., Iran, 2015